NAVAL POSTGRADUATE SCHOOL
Monterey, California

THESIS

AN EXPERIMENTAL INVESTIGATION OF THE GEOMETRIC CHARACTERISTICS OF FLAPPING-WING PROPULSION FOR A MICRO AIR VEHICLE

by

Jason Papadopoulos

June 2003

Thesis Advisor: Kevin D. Jones
Co-Advisor: Max F. Platzer

Approved for public release; distribution is unlimited.

THIS PAGE INTENTIONALLY LEFT BLANK

REPORT DOCUMENTATION PAGE			Form Approved OMB No. 0704-0188
Public reporting burden for this collection of information is estimated to average 1 hour per response, including the time for reviewing instruction, searching existing data sources, gathering and maintaining the data needed, and completing and reviewing the collection of information. Send comments regarding this burden estimate or any other aspect of this collection of information, including suggestions for reducing this burden, to Washington headquarters Services, Directorate for Information Operations and Reports, 1215 Jefferson Davis Highway, Suite 1204, Arlington, VA 22202-4302, and to the Office of Management and Budget, Paperwork Reduction Project (0704-0188) Washington DC 20503.			
1. AGENCY USE ONLY ***(Leave blank)***	**2. REPORT DATE** June 2003	**3. REPORT TYPE AND DATES COVERED** Master's Thesis	
4. TITLE AND SUBTITLE: An Experimental Investigation of the Geometric Characteristics of Flapping-Wing Propulsion for a Micro Air Vehicle			**5. FUNDING NUMBERS**
6. AUTHOR(S)			
7. PERFORMING ORGANIZATION NAME(S) AND ADDRESS(ES) Naval Postgraduate School Monterey, CA 93943-5000			**8. PERFORMING ORGANIZATION REPORT NUMBER**
9. SPONSORING /MONITORING AGENCY NAME(S) AND ADDRESS(ES) N/A			**10. SPONSORING/MONITORING AGENCY REPORT NUMBER**
11. SUPPLEMENTARY NOTES The views expressed in this thesis are those of the author and do not reflect the official policy or position of the Department of Defense or the U.S. Government.			
12a. DISTRIBUTION / AVAILABILITY STATEMENT Approved for public release; distribution is unlimited.			**12b. DISTRIBUTION CODE**

13. ABSTRACT ***(maximum 200 words)***

The geometric characteristics of flapping-wing propulsion are studied experimentally through the use of a force balance and a Micro Air Vehicle (MAV) system. The system used is built to duplicate the propulsion system currently on the flying model of the Naval Postgraduate School (NPS) MAV model. Experiments are carried out in a low speed wind tunnel to determine the effects of mean separation and plunge amplitude on the flapping wing propulsion system. Additionally, the effects of flapping-wing shape, flapping frequency, and MAV angle of attack (AOA) are also investigated. Some flow visualization is also performed. The intent is to optimize the system so that payload and controllability improvements can be made to the NPS MAV.

14. SUBJECT TERMS Micro Air Vehicle, Flapping-Wing Propulsion, Force Balance, Flow Visualization			**15. NUMBER OF PAGES** 89
			16. PRICE CODE
17. SECURITY CLASSIFICATION OF REPORT Unclassified	**18. SECURITY CLASSIFICATION OF THIS PAGE** Unclassified	**19. SECURITY CLASSIFICATION OF ABSTRACT** Unclassified	**20. LIMITATION OF ABSTRACT** UL

NSN 7540-01-280-5500 Standard Form 298 (Rev. 2-89)
Prescribed by ANSI Std. 239-18

THIS PAGE INTENTIONALLY LEFT BLANK

Approved for public release; distribution is unlimited.

AN EXPERIMENTAL INVESTIGATION OF THE GEOMETRIC CHARACTERISITCS OF FLAPPING-WING PROPULSION FOR A MICRO-AIR VEHICLE

Jason N. Papadopoulos
Ensign, United States Navy Reserve
B.S. Mechanical Engineering, University of Texas, 2002

Submitted in partial fulfillment of the
requirements for the degree of

MASTER OF SCIENCE IN AERONAUTICAL ENGINEERING

from the

NAVAL POSTGRADUATE SCHOOL
June 2003

Author: Jason Papadopoulos

Approved by: Dr. Kevin Jones
Thesis Advisor

Dr. Max Platzer
Co-Advisor

Dr. Max Platzer
Chairman, Department of Aeronautics and Astronautics

THIS PAGE INTENTIONALLY LEFT BLANK

ABSTRACT

The geometric characteristics of flapping-wing propulsion are studied experimentally through the use of a force balance and a Micro Air Vehicle (MAV) system. The system used is built to duplicate the propulsion system currently on the flying model of the Naval Postgraduate School (NPS) MAV model. Experiments are carried out in a low speed wind tunnel to determine the effects of mean separation and plunge amplitude on the flapping wing propulsion system. Additionally, the effects of flapping-wing shape, flapping frequency, and MAV angle of attack (AOA) are also investigated. Some flow visualization is also performed. The intent is to optimize the system so that payload and controllability improvements can be made to the NPS MAV.

THIS PAGE INTENTIONALLY LEFT BLANK

TABLE OF CONTENTS

LIST OF FIGURES

THIS PAGE INTENTIONALLY LEFT BLANK

ACKNOWLEDGMENTS

The author would like to express his sincerest gratitude to Dr. Kevin Jones for his time and efforts supervising and assisting in the completion of this project. Additionally, he would like to thank Dr. Max Platzer for his oversight and encouragement.

The author would also like to thank Professor Art Schoenstadt for his aid in the creation of the MATLAB codes used for this paper.

Finally, the author would like to thank his family for their continuing support and encouragement throughout the years, without whom this would not have been possible.

THIS PAGE INTENTIONALLY LEFT BLANK

I. INTRODUCTION

A. OVERVIEW

This paper examines the geometric characteristics of a flapping-wing Micro Air Vehicle (MAV) propulsion system in order to determine their effects on the lift and thrust produced by the system. This study builds on work that has been carried out over the past several years at the Naval Postgraduate School (NPS). The ultimate goal of this paper is to aid in the research and development of a flight worthy, remote-controlled MAV.

All experiments were carried out in the NPS 1.5 m x 1.5 m wind tunnel. The MAV models used in the experiments were chosen to closely imitate the construction of the MAV model developed at NPS that has already demonstrated capability for controlled flight. In order to obtain lift and thrust measurements the propulsion system was sting mounted through the floor of the wind tunnel and connected to a force balance. Professor Kevin Jones previously developed all of the MAV component parts as well as the force balance. Finally, some flow visualization experiments were carried out to help understand flow behavior.

B. BACKGROUND

In 1997, the Defense Advanced Research Projects Agency (DARPA) became interested in the possibility of using MAVs in military operations; their inherent ability for reconnaissance and surveillance missions being the primary focus. DARPA's specifications for the MAV were that it be, "an affordable, fully functional, military capable, flight

vehicle, limited to 15 cm in length, width or height." [Ref. 1]. Additionally, it was required that the MAV be able to sustain flight times of at least 20 minutes, have a range of 10 km, and a payload capability of 20 grams.

The war in Afghanistan made the need for a flight capable MAV even more apparent. The perilous job of searching caves for hostile activity could have been accelerated while at the same time reducing personnel risks to soldiers on the ground. The capability of an advanced warning system using MAVs to locate snipers and enemy positions would have greatly aided soldiers in an urban combat environment. Additionally, the CIA had also expressed interest in employing MAVs in a variety of different surveillance missions.

Many of the MAV designs developed in response to the DARPA request attempted to utilize a propeller for thrust generation. Propeller driven aircraft such as the *Black Widow* MAV [Ref. 2], shown in **Figure 1,** met many of DARPA's initial requirements but had some major drawbacks. These disadvantages included high flight speeds that inhibit maneuverability in confined spaces, and noise generation from the propeller.

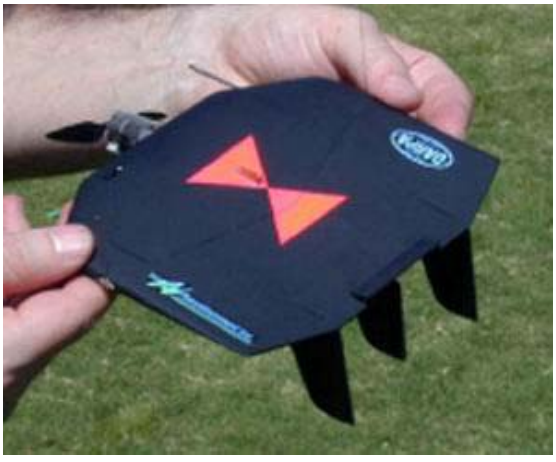

Figure 1. Black Widow MAV

Another prominent design idea for the MAVs was bio-mimicry. One popular example seen here in **Figure 2** is the AeroVironment *Microbat* [Ref 3]. The idea to imitate nature is a logical one as insects and birds have proved very adept at flying. However, evolution is constrained by the initial conditions of the process. For example, a four-legged creature will not develop a propeller, but instead delegate its appendages to a flight-producing role. Thus, it is possible that evolution might have missed a few solutions to the problem of flight.

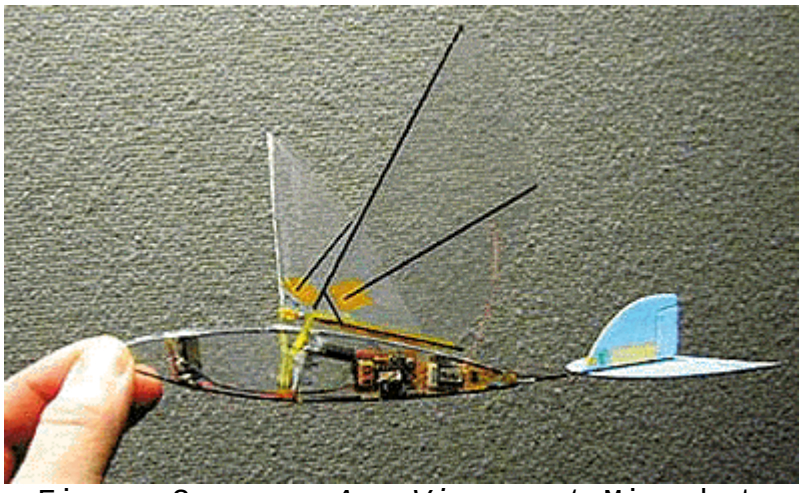

Figure 2. *AeroVironment* Microbat

C. FLAPPING-WING PROPULSION

The use of a flapping wing to create thrust was first explained in the early 20th century by two independent researchers. Knoller in 1909 [Ref. 4] followed by Betz in 1912 [Ref. 5] each perceived that flapping a wing in a free stream flow resulted in an effective angle of attack with a normal force vector containing both lift and thrust components. This phenomenon is now referred to as the Knoller-Betz effect and is displayed in **Figure 3.**

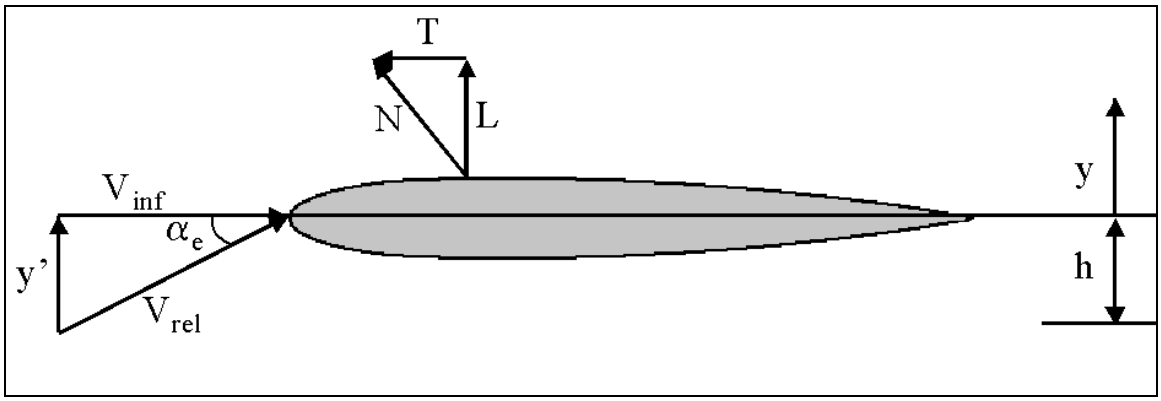

Figure 3. Knoller-Betz Effect

In 1922, Katzmayr [Ref. 6] conducted wind tunnel tests to validate the Knoller-Betz effect. Rather than flapping the airfoil, Katzmayr sinusoidally oscillated the freestream velocity. Katzmayr's measurements conclusively proved that an airfoil mounted in an oscillating wind stream experienced a thrust force. Also adding to this increasing field of research was Prandtl's student Birnbaum [Ref. 7 & 8]. Birnbaum developed a solution for incompressible flow past flapping airfoils and observed the conditions that lead to flutter or thrust generation. He also suggested the flapping-wing as an alternative to the propeller.

In the mid 1930's Karman and Burgers [Ref. 9] sought to explain the theory behind whether thrust or drag was produced by a flapping wing. They were joined by Garrick [Ref. 10] in 1936, who employed Theodorsen's theory to examine the problem of sinusoidally plunging and/or pitching airfoils. In the 1940's and 50's, Schmidt [Ref. 11] strove to improve efficiency of flapping wing propulsion by employing two airfoils in tandem, one behind the other. Schmidt's research resulted in the creation of

the *wave propeller* (**See Figure 4**), which he claimed achieved efficiencies as good as those of conventional propellers.

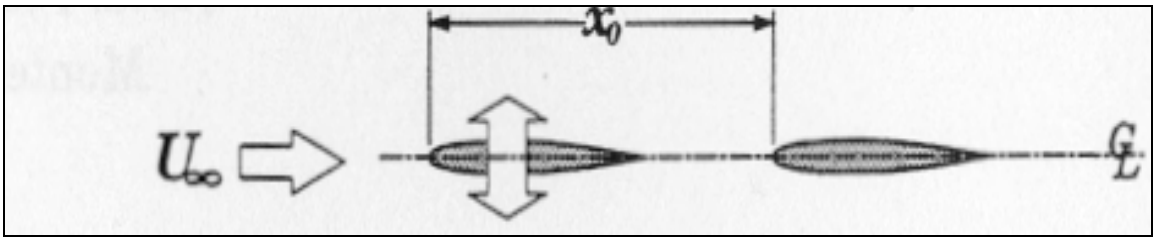

Figure 4. Wave Propeller Setup

More recently, Jones and Platzer [Ref 12 & 13] studied Schmidt's wave propeller and also examined other wake interference configurations. The most promising of these configurations was the opposed plunge configuration shown in **Figure 5**. The opposed plunge configuration attempted to produce and take advantage of ground-effect conditions similar to when a bird flies close to the water's surface. Its many benefits included being mechanically and aerodynamically balanced, as well as producing greater thrust than the wave propeller configuration. In the last few years, Jones and Platzer have customized the opposed plunge configuration to be used as the propulsion system for a MAV they developed [Ref. 13]. The first sustained flight took place in December of 2003, and further research into controllability and durability issues is currently being studied.

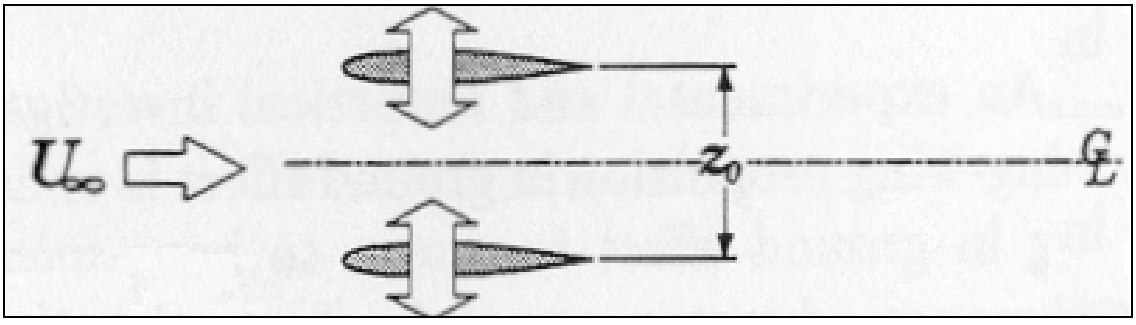

Figure 5. Opposed-Plunge Setup

The standard configuration studied in this paper attempts to imitate as closely as possible the actual configuration of the current flying MAV model (**See Figure 6**). All changes made to the standard configuration are aimed at determining the effect on performance of the flying MAV.

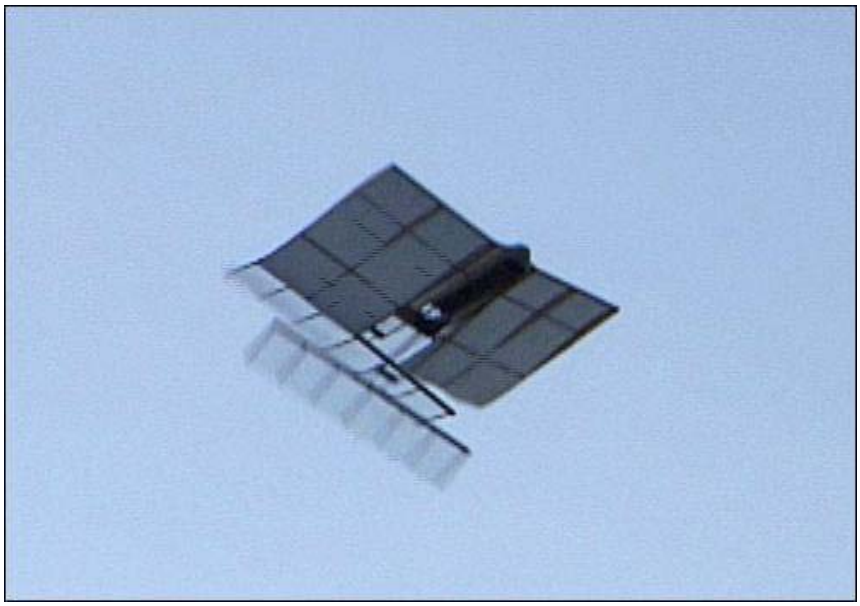

Figure 6. NPS Prototype MAV

II. EXPERIMENTAL SETUP

A. PROPUSLION SYSTEM

The motor used to drive the NPS MAV is 1.2 volt pager motor that is run at 5 volts to increase power density. The lifespan of small motors under these conditions are not conducive to prolonged experimental analysis because of brush wear problems. Consequently, the propulsion system used during experimentation incorporated a Faulhaber direct current motor with an independent power source. It was powered by an ELENCO MX-9300 Power Supply from which the voltage into the motor was varied. The shaft speed of the motor was slowed down using a 37:1 planetary gear system. With this gear ratio, the frequency of the rotating shaft powering the flapping wings could be made to closely mimic those found in the actual MAV models.

A resistor with a 0.011 ohm resistance was placed in series with the motor in order to measure the motor current. Since the drop in voltage across the resistor was negligible compared to the voltage drop across the motor, the motor voltage reading was unaffected. However, an amplifier was needed to add a fixed gain to the voltage drop across the resistor so it could be read accurately by the data acquisition system. The voltage drop across the resistor was later converted to current when the data was analyzed. Both the motor voltage and the voltage drop representing the motor current were fed into the data acquisition system. A circuit block was built to facilitate the connection of leads to the motor circuit. A diagram of the motor circuit can be seen in **Figure 7**.

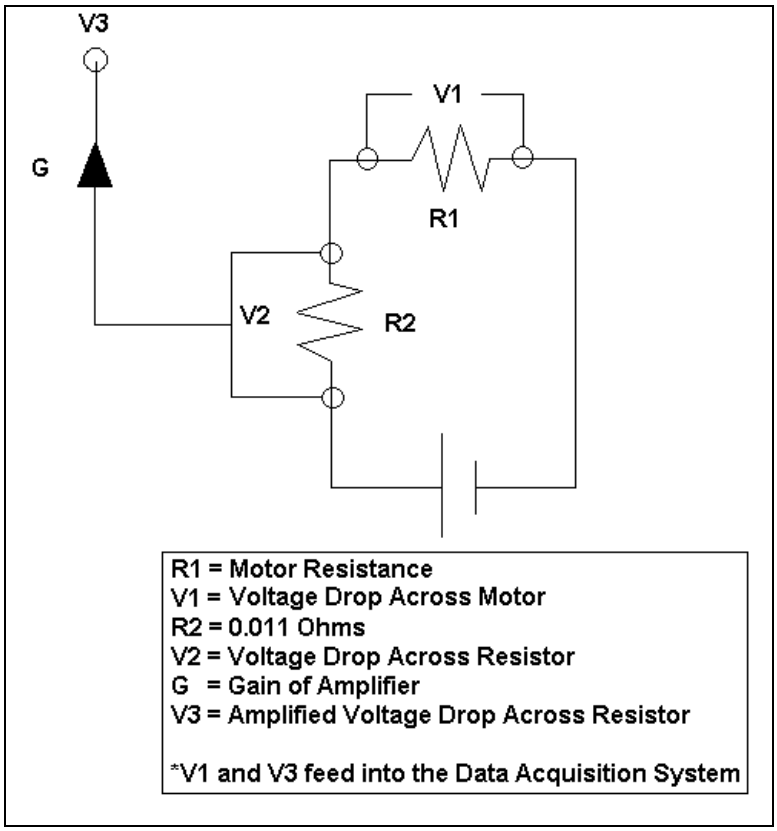

Figure 7. Motor Circuit Schematic

In order to measure the propulsion shaft speeds, an aluminum disk containing a notch was placed onto the slowed down shaft. A light beam whose path was interrupted by the disk could only strike a photosensitive diode when the notch was lined up with the light beam. This diode completed a circuit that had a fixed voltage. When the shaft rotated, the effect was that the voltage in the diode's circuit had the form of a square wave. This voltage was fed into a signal conditioner and then into the data acquisition system. The speed of the shaft powering the flapping wings was found by using the sample rate of the data acquisition system to determine the time from the

start of one square wave to the next. The square wave was also fed into an oscilloscope to allow for real-time frequency readings.

A crankshaft was used to change the rotational motion of the shaft into linear movement. Connecting rods linked the crankshaft to a set of flapping beams that produced the desired motion. The size of the crankshaft and connecting rods governed the plunge amplitude and mean separation of the wings. The flapping beams were screwed on the front end to a composite case that contained the motor and gear system, while the flapping wings were attached to the other end. The leading edge of the flapping wing was cylindrical with tapered ends and constructed from a thin dowel of balsa wood. The rest of the wing surface was lightweight plastic laminate. Support ribs made from carbon-fiber ran from the leading edge to the trailing edge of these wings. The wings were super-glued to the flapping beams via a thin carbon fiber strip. The stiffness of this strip governs the pitch angle oscillations found in the wing and allow for a passive feathering mechanism [Ref. 14]. A picture of the complete propulsion system can be seen in **Figure 8**. Dr. Kevin Jones built all MAV components, and further details on the construction of these parts can be found in reference 13.

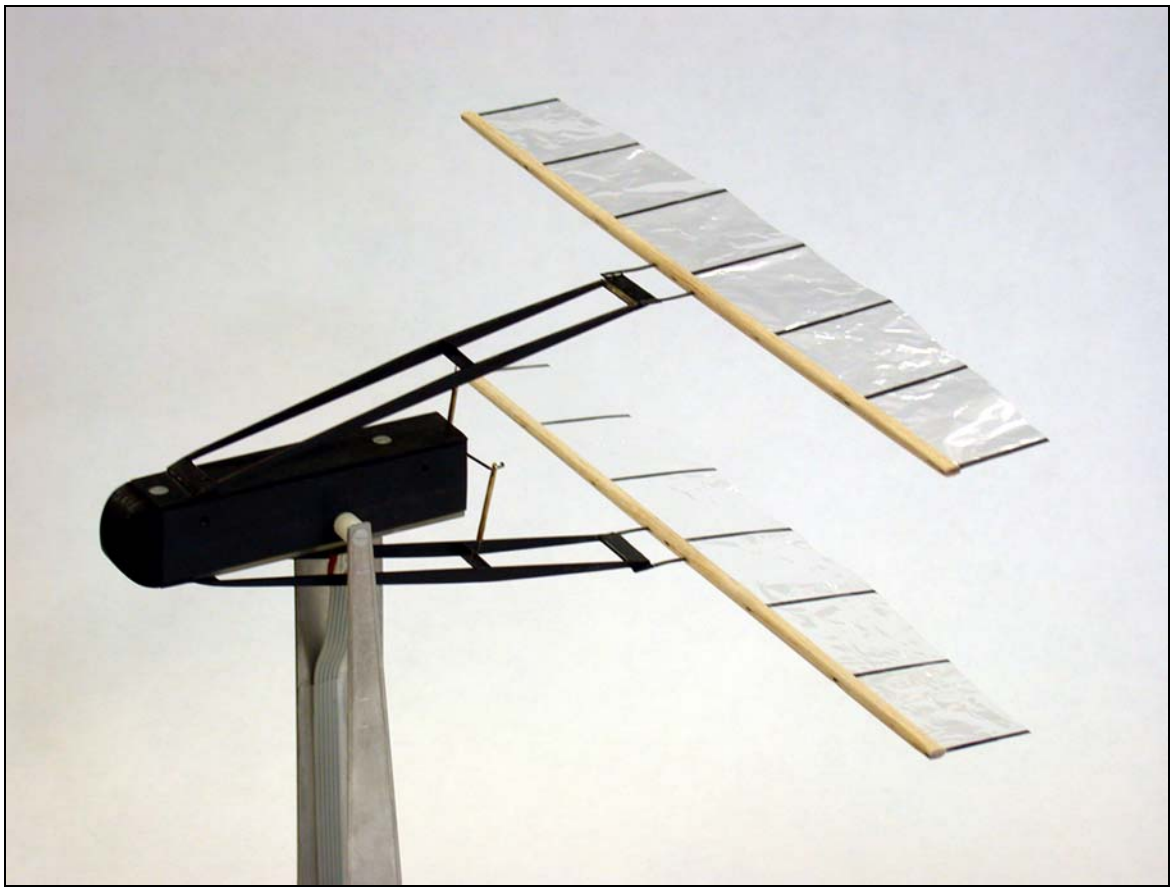

Figure 8. Test Model Propulsion System

B. FORCE BALANCE

The entire propulsion system was sting-mounted upon a force balance to measure the lift and thrust being produced by the model. Dr. Kevin Jones designed the force balance to utilize moment-arm principles to magnify the extremely small forces being produced by the flapping wings. Load cells were used to translate these forces into voltages that were then fed into the data acquisition system. The load cells used were Omega LC703-025 miniature low profile tension/compression links.

The force balance was mounted through the floor of the NPS wind tunnel and connected underneath to an immobile stand. The stand was independent of the wind tunnel and

prevented any vibrations of the wind tunnel walls from corrupting the force balance readings. The distance from the floor of the wind tunnel to the bottom of the model was measured to be two feet. This placed the flapping wings near the center of the wind tunnel test section, but allowed for laser Doppler velocimetry (LDV) above the centerline.

C. WIND TUNNEL

All experimentation was conducted in the NPS low-speed wind tunnel illustrated in **Figure 9**. The wind tunnel has a 4.5m x 4.5 m square inlet that converges to a 1.5m x 1.5m test section. Tunnel speeds vary from 0 to 9.5 m/s, and are controlled by a variable pitch fan powered by a constant speed electric motor. Rubber sleeves are used to isolate the vibrations of the fan assembly from the test section.

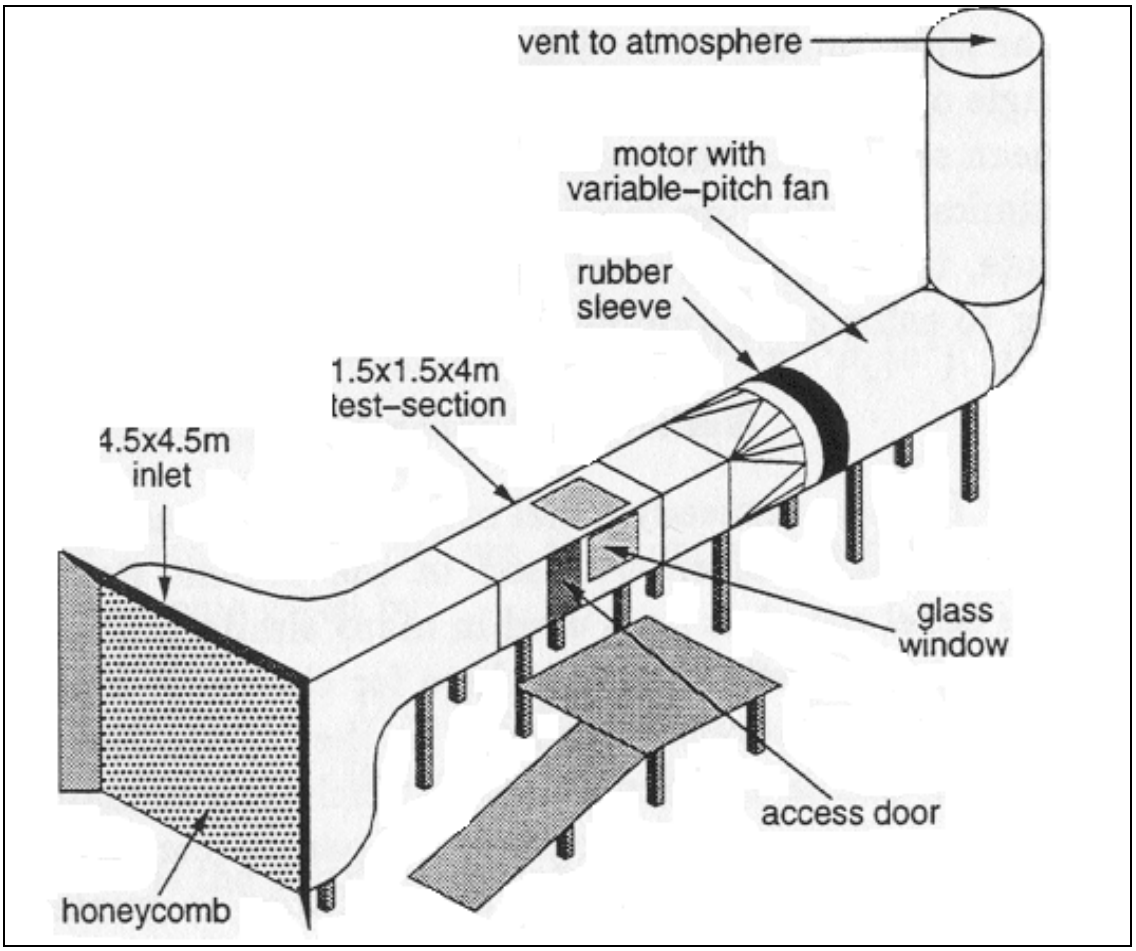

Figure 9. Schematic of NPS Low-Speed Wind Tunnel

During experimentation a pitot-static tube was used to determine the tunnel velocity. The pitot tube was located directly above the model, and approximately 1.5 feet below the ceiling of the test section. A MKS Baratron type 223B differential pressure transducer took the pressure seen by the pitot tube, and converted it to a voltage which was read by a Metex 3610D digital multimeter. The tunnel speed was calculated using Bernoulli's equation and the conversion ratio of the pressure transducer (1 volt per 133.2 Pa).

D. DATA ACQUISITION SYSTEM

All of the signal lines from the propulsion system and force balance were fed into an Omega Screw Terminal Block. The signals wired into the block based on their channel number location were:

Channel 1: Rotary Encoder

Channel 2: Lift from Force Balance

Channel 3: Thrust from Force Balance

Channel 5: Motor Voltage

Channel 6: Motor Current

The pressure transducer voltage was initially supposed to be wired as Channel 4 so that real-time velocity measurements could be taken. However, all attempts to hook up the pressure transducer to the screw terminal block (in Channel 4 and other locations as well) resulted in ground loop problems and cross-talk between the channels. Without the transducer hookup, no interference was seen between the channels. Thus, the transducer velocity was read from the multimeter directly, and Channel 4 was left unused.

The data acquisition card used in our experiments was an Omega DAQP-16-OM-A Type II PCMCIA card. It had an effective range of +/- 10 volts and used twos complement 16-bit precision to read and store the data. The card was hooked directly to a laptop PC and was controlled using the program DaqEZ Version 4.11. Using this program the sample rate and duration of each measurement could be controlled, and the data files stored directly to the laptop hard drive. A schematic summarizing the complete setup can be seen in **Figure 10**.

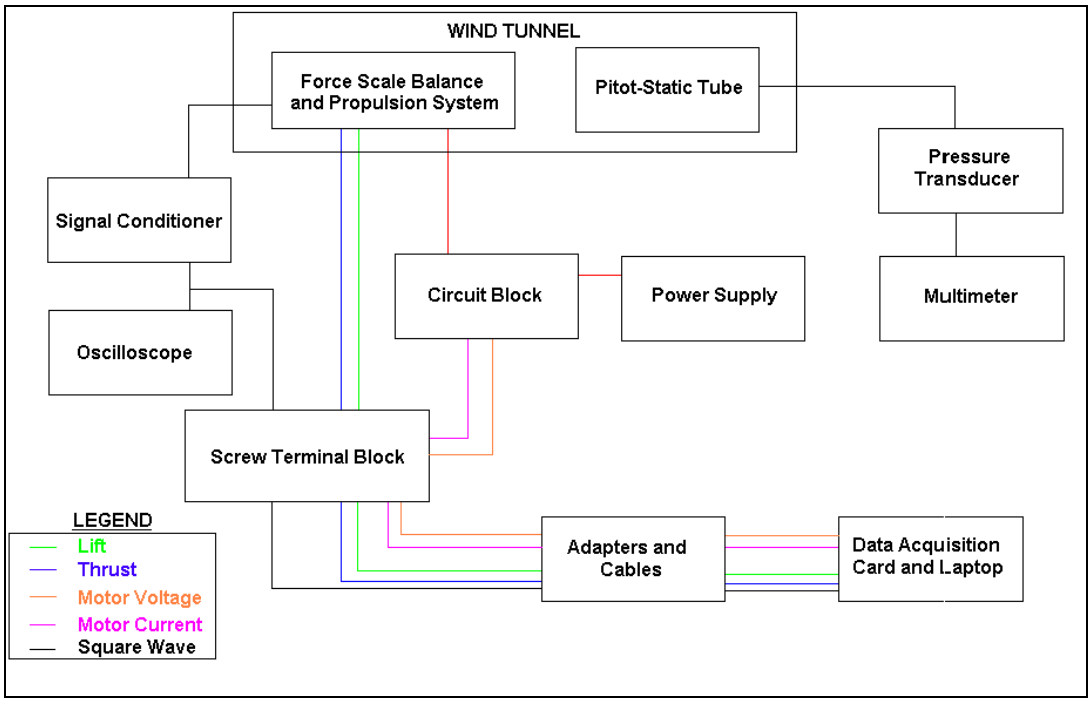

Figure 10. Schematic of Experimental Setup

III. EXPERIMENTAL ANALYSIS

A. CALIBRATION

1. Lift

A calibration was required to determine the conversion ratio from the twos complement integers outputted by the data acquisition system to the force in Newtons produced in the vertical direction. The procedure for the calibration of lift consisted of placing a series of known masses directly on top of the force balance main body. Five samples were taken of each mass, recording the lift and thrust force seen by the balance. These five samples were then referred to as the data set for that particular configuration. A sample rate of 2000 hz and a test time of 10 seconds was specified using the DaqEZ software. Additionally, data was collected with no mass atop the force balance to obtain a zero reference reading that would be subtracted from all of the samples in all of the data sets.

Next, the average lift in twos complements units was taken for each of the five samples in each of the nine data sets. These points were then plotted against the force in Newtons exerted upon the balance by each point. A linear regression was then performed to obtain the slope of the line that best fit the data. The line had the form

$$y = A + Bx \tag{1}$$

where y was the lift in Newtons, and x was the lift reading. The slope was calculated as

$$B = \frac{N(\Sigma x_i y_i) - (\Sigma x_i)(\Sigma y_i)}{N(\Sigma x_i^2) - (\Sigma x_i)^2} \tag{2}$$

The y-intercept was calculated to aid in plotting the best fit line, but it was ignored in the actual analysis because the offset changed daily depending on atmospheric conditions. This problem was overcome by determining the offset every day that experiments were performed. The offset was established by taking a zero data set at the beginning and end of each data set. The final equation which governed the conversion of lift in twos complement units to lift in Newtons had the form

$$y = offset + (1.5651\text{e-}4)x \qquad (3)$$

Additionally, the error in the slope determined in equation (3) was also found. This error was calculated based upon the uncertainty in the measurements used to obtain the average value found for each data set. The uncertainty in the average values was measured as

$$\sigma_y^2 = \frac{1}{N-2}\sum_{i=1}^{N}(y_i - A - Bx_i)^2 \qquad (4)$$

and the uncertainty in the slope, B, was measured as

$$\sigma_B^2 = \frac{N\sigma_y^2}{N(\Sigma x_i^2) - (\Sigma x_i)^2} \qquad (5)$$

These uncertainties were later used in the error analysis. A plot of the best-fit line and the adjusted error lines can be seen in **Figure 11**. The adjusted error lines are in red.

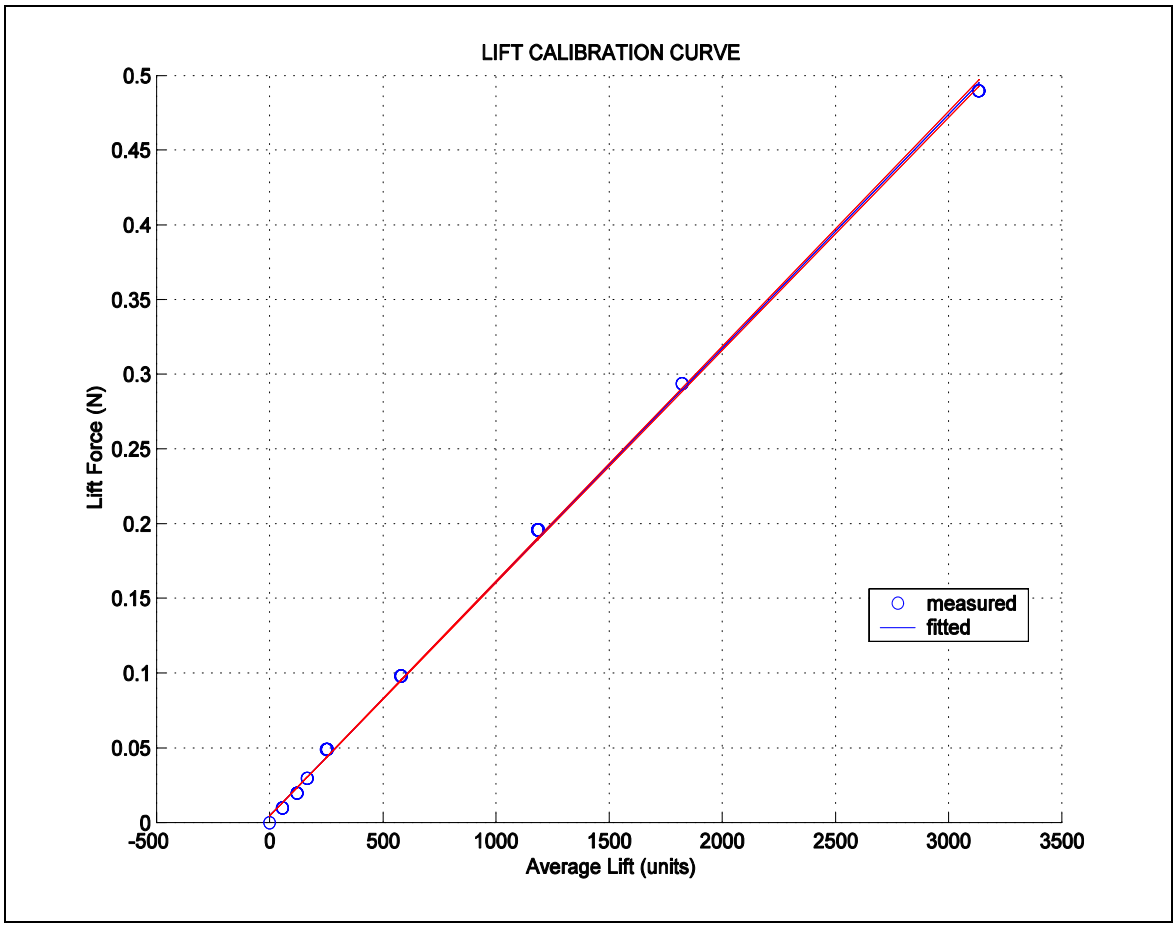

Figure 11. Lift Calibration Curve

Lastly, a plot was made of the average thrust force in twos complement units versus the average lift force in twos complements units (**See Figure 12**). This graph represented the cross talk between the lift and thrust components on the force balance. The total vertical difference between the highest and lowest value of the thrust was divided by two and used as the error estimate in the thrust channel as a result of lift forces.

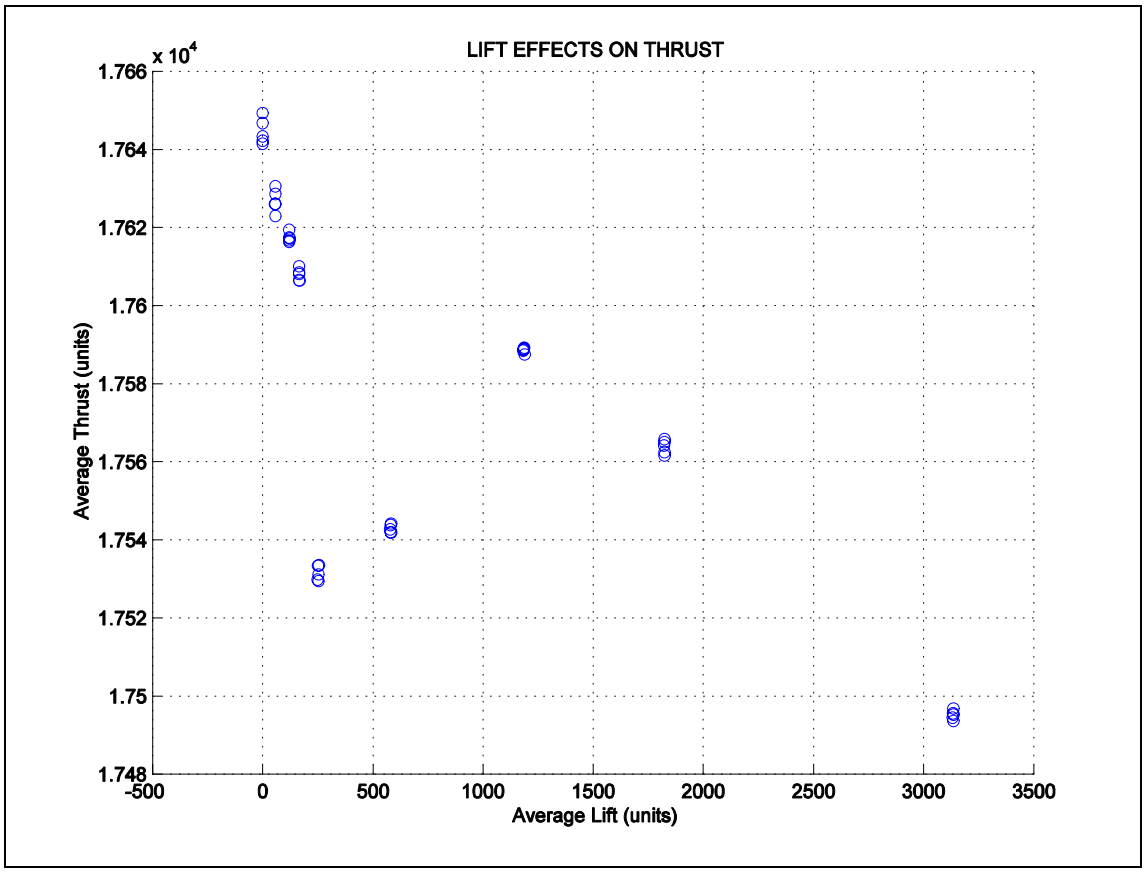

Figure 12. Lift Channel Interference on Thrust Channel

2. Thrust

The conversion of thrust from twos complement units to Newtons was nearly identical to the lift conversion. The main difference between the two lay in the setup. In order to generate horizontal forces of a known magnitude a string was attached to the sting mounted propulsion system. This string ran over a pulley and had a mass tied to the opposite end. Care was taken to insure that the string remained horizontal until it reached the pulley so that cross talk in the lift direction would be minimized. A series of masses identical to those used in the lift calibration were then hung on the opposite end of the string. Both the thrust and lift data was recorded and

again, five samples were taken with each mass using the same sample rate and test time as the lift calibration.

The techniques used to analyze the thrust data sets were identical to those used in the lift calibration. Averages were taken for each data set and plotted against the true thrust force in Newtons. A best-fit line was fitted to this plot using the same formulas as shown in equations (1) and (2). The only difference was that this time the variable *y* represented the thrust in Newtons, and *x* represented the thrust in twos complement units. The final equation that governed the conversion of thrust into Newtons was given by

$$y = \text{offset} + (5.7349e - 5)x \qquad (6)$$

The y-intercept was again ignored and calculated whenever experiments were conducted. The error in the slope was computed using equations (4) and (5), and the adjusted lines were plotted against the best-fit line (**See Figure 13**). The error in the thrust calibration curve was again taken as the maximum difference between any of these lines.

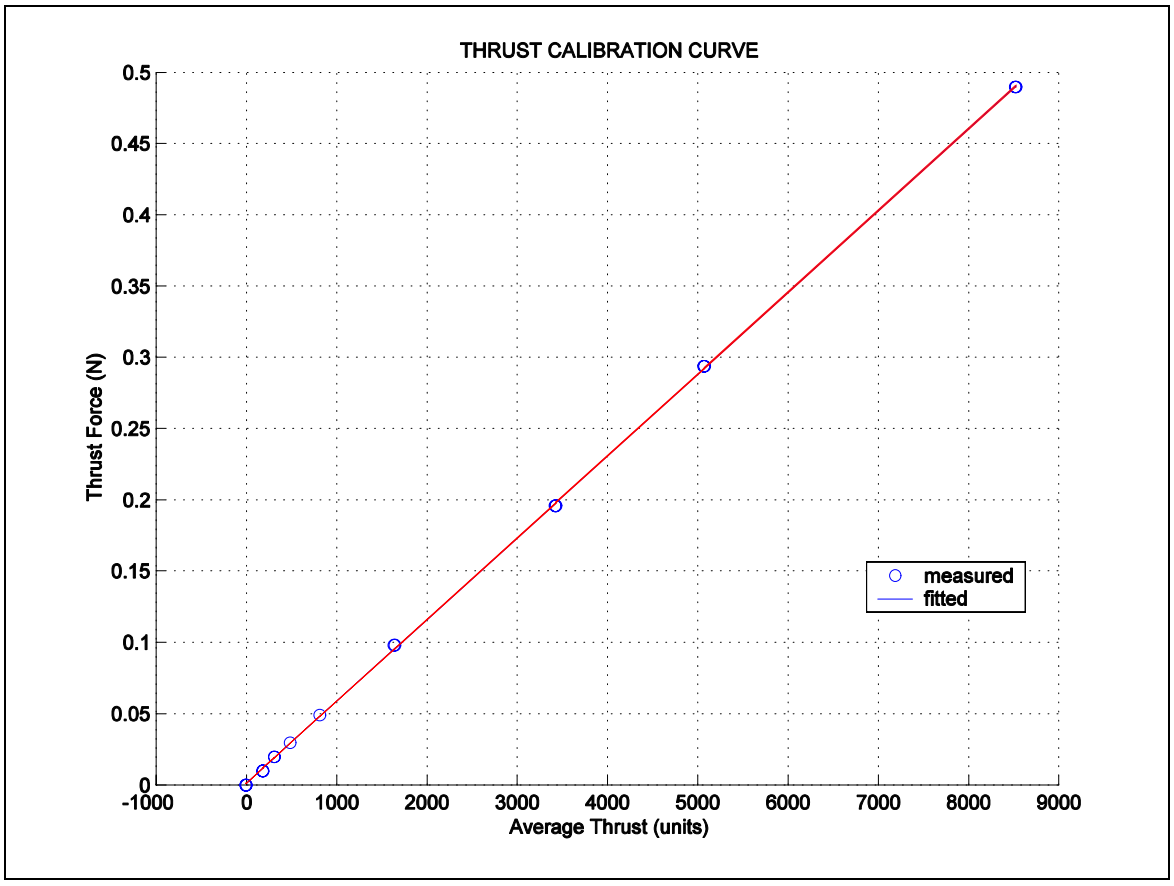

Figure 13. Thrust Calibration Curve

Finally, a plot of the interference of the thrust force on the lift was created, and an estimate of the error in the lift force due to thrust was obtained (**See Figure 14**).

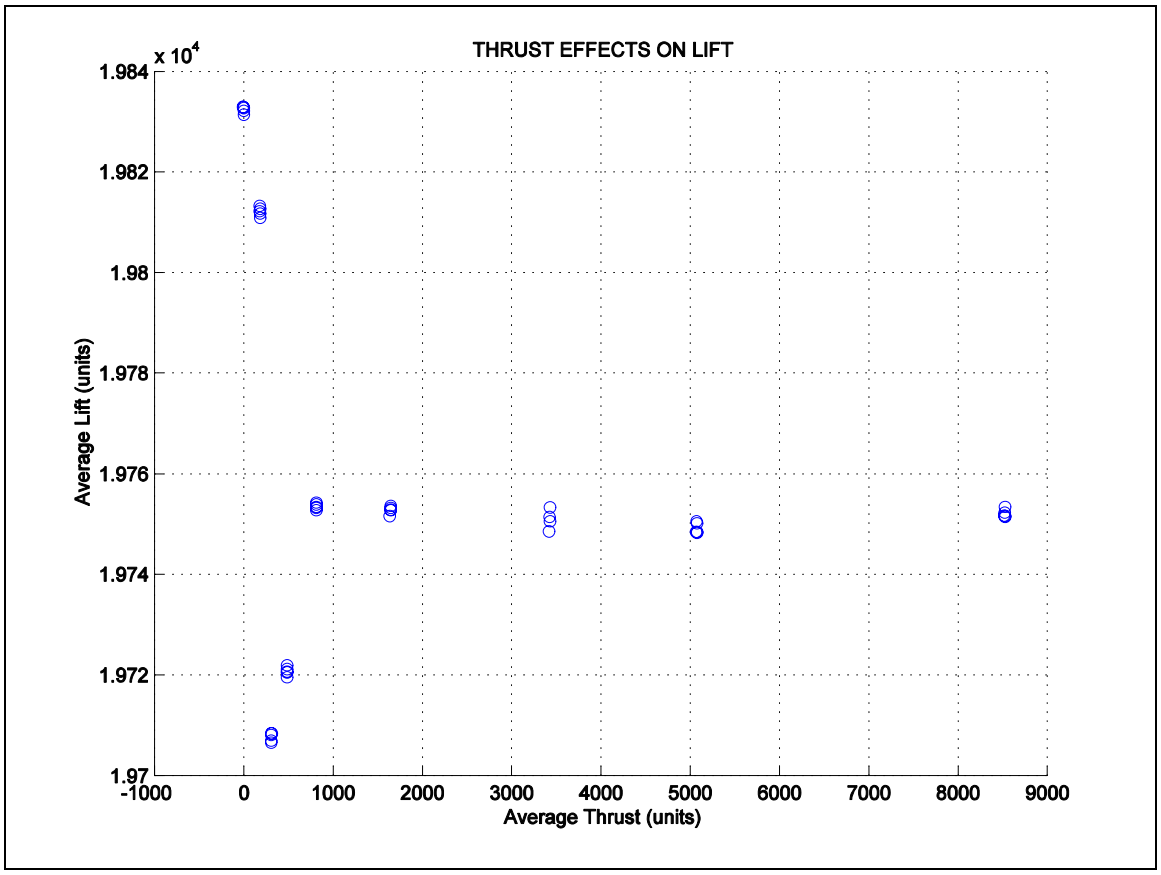

Figure 14. Thrust Channel Interference in Lift Channel

3. Motor Voltage and Motor Current

The motor voltage calibration was purely analytical. Because the input channels were all voltage readings, the only adjusting needed was to find the conversion for the motor voltages that were recorded as twos complement units. Given that the data acquisition card had 16-bit precision, and that the range of the card was specified at +/- 10 volts, the conversion from twos complement units to volts could be calculated. The conversion ratio was determined to be

$$(3.05185e-4)\frac{volts}{unit} \qquad (7)$$

The motor current read by the data acquisition system was actually the amplified voltage drop across a small resistor (**See Figure 7**). The gain on the amplifier was unknown so a calibration test was needed. During calibration a known resistance replaced the motor and a fixed voltage was passed through the circuit. The voltage drop across the small resistor was calculated and compared to the voltage coming out of the amplifier. The ratio of the two was the gain given to the signal. This process was repeated using three different resistances to replace the motor. The average of these three trial runs was used as the gain on the amplifier, and the standard deviation was used as the approximate error in the gain. The gain was calculated to be 256. With this value for the gain, the conversion of twos complement units to volts representative of the current was calculated to be

$$(1.9005e-6)\frac{volts}{unit} \qquad (8)$$

These voltages were then divided by the resistance of the small resistor, 0.011 ohms, to give the actual current in amperes running through the motor.

4. Motor Shaft Power

The mechanical power produced by the motor and gear-drive assembly was needed to calculate meaningful efficiencies. In order to determine this power a special setup was needed. The wings, flapping beams, and all other associated parts were removed from the propulsion system. A spindle was then attached to the motor shaft and a very thin (0.005” diameter) copper wire super-glued to the spindle. The wire ran up and over a pulley approximately two feet above the motor shaft and then down four feet to the floor. A series of different masses were hung from the

copper wire and data sets were taken while the motor wound up the wire and raised the mass. Each mass was wound up using an increasing set of motor voltages.

The shaft-power was calculated as rotational shaft speed multiplied by the shaft torque. The shaft torque was the weight of the mass tied to the string multiplied by the sum of the radius of the spindle and half a thread width. The calculation of the shaft rotational speed is explained in the experimental setup.

The data from the calculations showed that the masses below thirty grams were indistinguishable from one another; all seemed to require the same amount of input power from the motor. Clearly this was incorrect, as the current should increase with mass for a given voltage. Therefore, the readings below thirty grams were omitted, and a cubic interpolation was attempted based on the sparse data of the upper three readings, and a zero set (**See Figure 15**). The zero set assumed that the current was nearly zero (0.01 amperes) regardless of the range, and that the shaft power was zero.

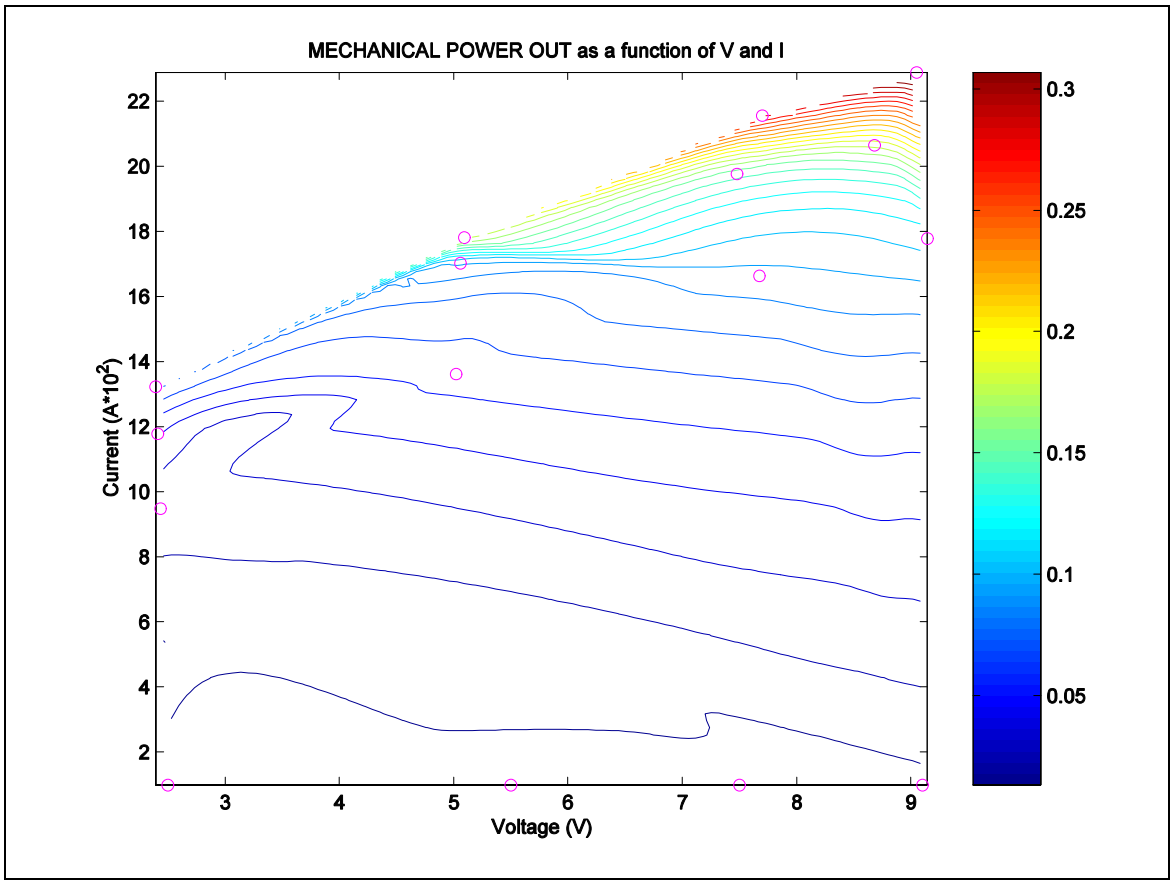

Figure 15. Mechanical Power From Test Motor

Initially the interpolation seemed reasonable, however, later testing and analysis showed that the values specified in **Figure 15** were too low to be accurate. The power output values from the graph were yielding figures of merit an order of magnitude greater than that produced by the test MAV. The problem was that by choosing an oversized motor, the motor friction was also increased. The torque necessary to overcome this friction was of the same magnitude of the torque necessary to flap the wings. Thus, the noise from the motor friction prevented accurate torque measurements in the lower regions. Unfortunately, this is the region in which the flapping wings operate. Therefore, **Figure 15** was determined to be inaccurate and

efficiency calculations were not performed using the large motor.

a. MAV Motor Shaft Power

The same setup used to calculate the motor shaft power of the propulsion system was also used to calculate the shaft power of the motor used in the flying MAV. However, with the MAV motor the problems of motor friction were not an issue due to its smaller size and design for lower voltages. As a result, accurate measurements were taken and the MAV motor shaft power as well as its efficiency was calculated (See **Figures 16 & 17**).

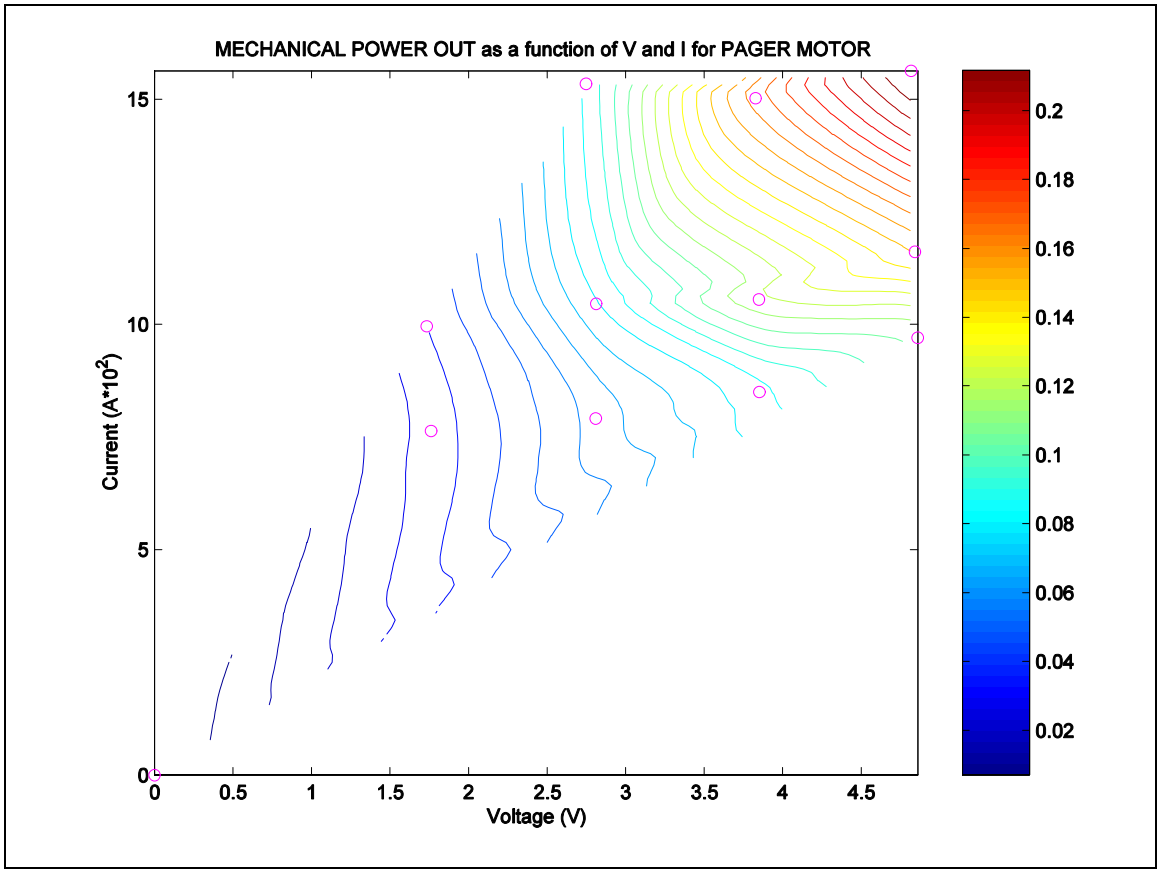

Figure 16. Mechanical Power From MAV Motor

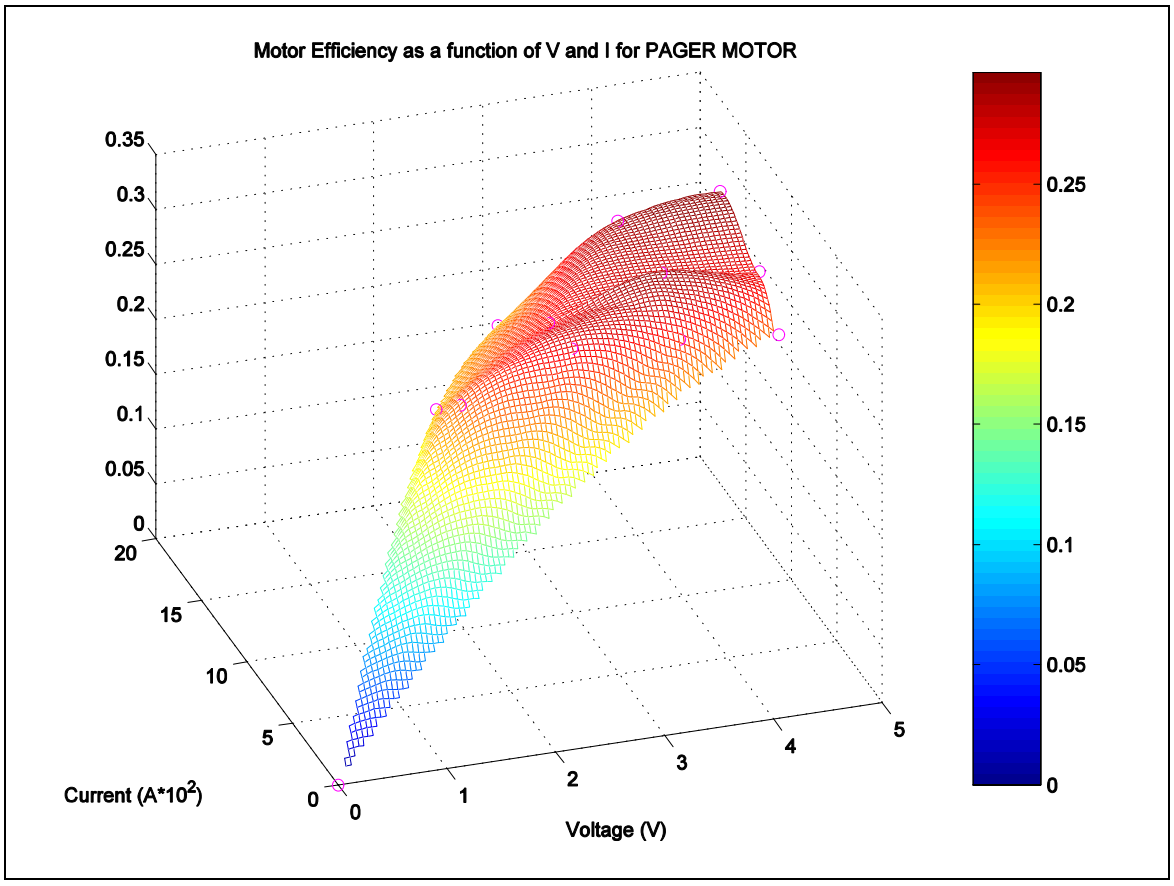

Figure 17. MAV Motor Efficiency

To date the only flying MAV model used a motor identical to the one tested here. That MAV was measured to draw 5 volts at approximately 0.3 amperes.

B. EXPERIMENTAL METHOD

1. Test Procedures

The same procedure was used for each geometric variant of the MAV components that were tested. First, the MAV components were setup on the sting connected to the force balance. Once the components were attached, the angle of attack (AOA) of the model was set to zero degrees. The AOA

was measured as the angle that the top surface of the fuselage made with the horizontal. The angle was measured using an angle finder.

Once the model was set to an AOA of zero degrees, the motor voltage was set to approximately 5 volts and a data set obtained. Each data set consisted of five samples measured with a sample rate of 2000 HZ for 10 seconds. The values measured in each data set were the 5 lines entering the data acquisition system discussed previously. The motor voltage was then increased incrementally from 5 volts to approximately 10 or 17 volts, with one data set taken at every voltage in between. Initially, 10 volts was set as the limit because of the range constraints of the DAQ card in reading the motor voltage. However, after it was discovered that efficiency could not be calculated, Channels 5 and 6 were disconnected and the motor was run at the higher voltages. These higher voltages yielded flapping frequencies similar to the flying MAV model.

Additionally, two data sets were obtained with no motor power, before and after all the other data sets had been taken. These two data sets were averaged and then used as the thrust offset value for the six data sets taken with the motor running. The total difference between the two offset data sets was used as the drift error for all of the motor voltage data sets they spanned.

After the last offset data set had been taken, the velocity of the wind tunnel was increased. The AOA was held constant and the entire process was repeated again for a new tunnel velocity. The tunnel velocities tested ranged from approximately 0–4 m/s. Once all of the tunnel

velocities had been tested for one particular AOA, the wind tunnel was shut down, a new AOA was set, and the entire process repeated.

The only difference between any of the samples taken involved the thrust offset data sets when the tunnel speeds were not zero. For these data sets the motor voltage was not set to 0 volts as described above, but instead to 0.7 volts. At 0.7 volts the flapping wings moved very slowly and created no effective thrust. This was done to account for the different profile drag characteristics of the flapping wings when they were at maximum and minimum separation. Since these offset values were used as the zero-reference conditions, the profile drag on the MAV was automatically removed from the thrust readings initially measured. Therefore, the thrust readings measured in the experiments were the net positive thrust of the MAV flapping wings.

2. Test Geometries

The first test model was built to duplicate as close as possible the current flying MAV built by Dr. Jones. Key aspects of its geometry and component materials, except for the motor and gear system, were identical to the flying MAV. The plunge amplitude, h, was measured to be 37.5% of the flapping wing chord. A diagram of this setup can be seen in **Figure 18** and will from here on out be referred to as the *Standard Model*.

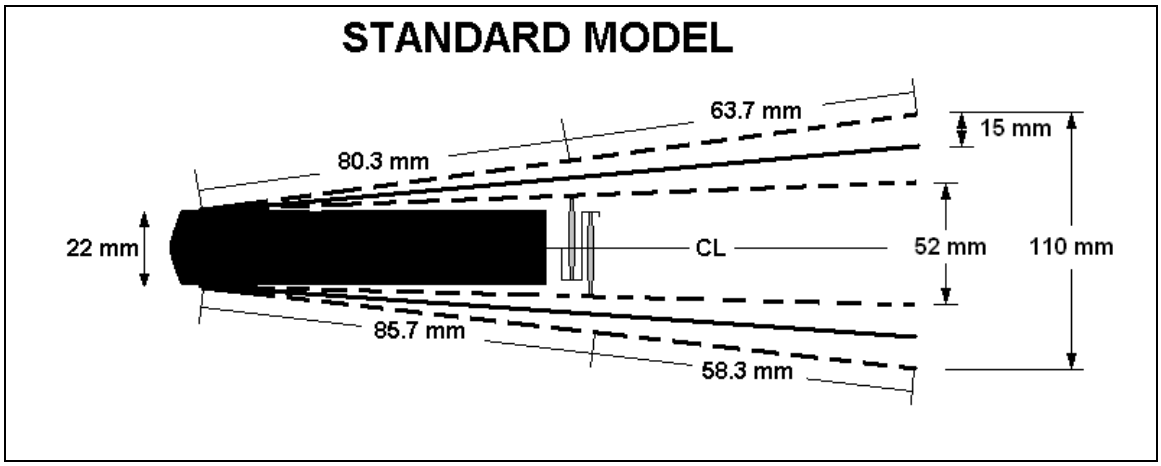

Figure 18. Standard Model Schematic

a. Standard Model

During previous flight tests with the MAV it was observed that when the flapping wings had a square design, teetering of the flapping wing leading edge occurred about its connection to the flapping beam. This problem was overcome by altering the construction of the flapping wings to a tapered design (**See Figure 19**). However, it was not clear whether the tapered wing had a detrimental effect on thrust production. For this reason, the *Standard Model* was fitted with both square and tapered, flapping wings, and wind tunnel tests performed on both configurations for comparison.

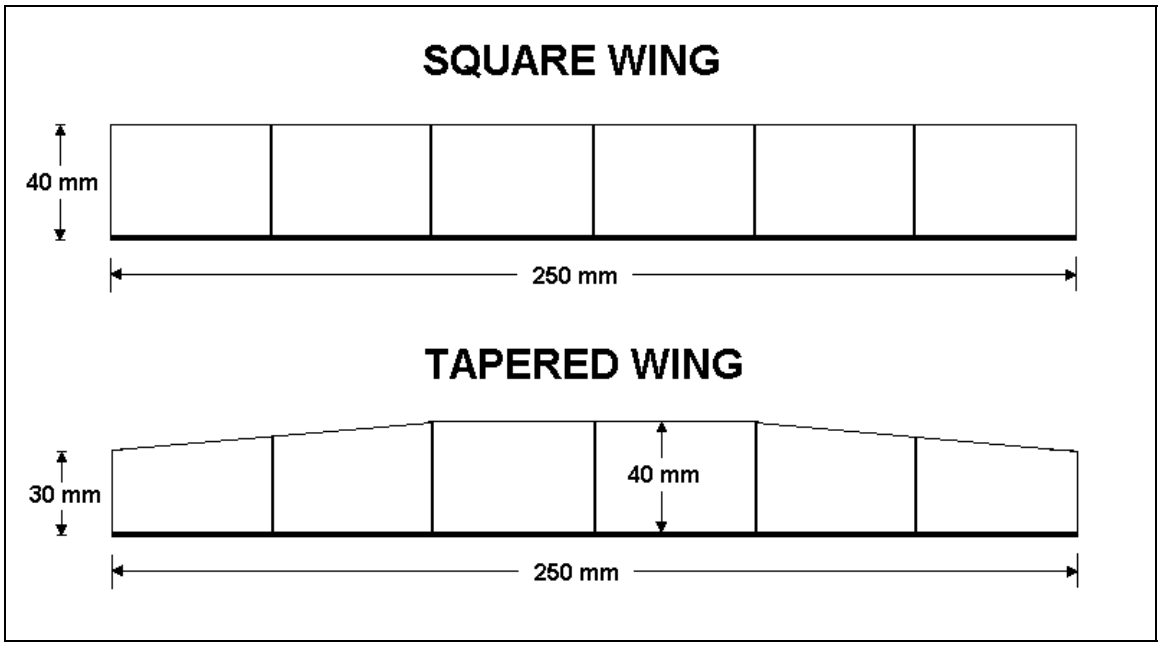

Figure 19. Flapping Wings Used in Experiments

After the above tests were completed, main wings were connected to the fuselage. The wings were identical in size and shape to the ones used on the flying MAV. The ribs were made from balsa wood and carbon fiber and the wing surface was Japanese tissue paper. The wings had a span of 270 mm, a chord length of 140 mm, and 8.5 degrees of dihedral. This configuration, the *Standard Model* with main wings, was now nearly identical to the flying MAV (**See Figure 20**). The only difference lay in the size of the fuselage needed to accommodate the larger motor and the associated weight. Wind tunnel tests were run on this configuration to act as a basis for comparison with later component modifications.

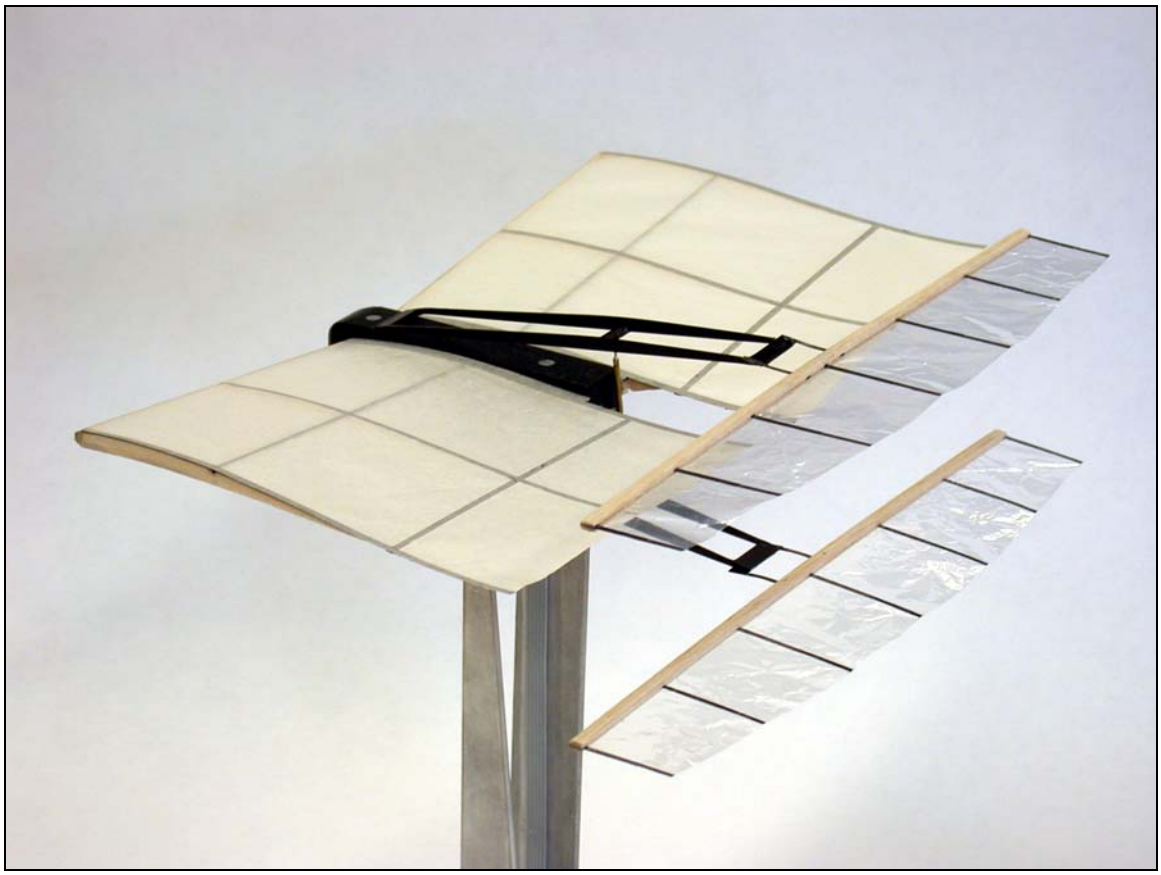

Figure 20. Standard Model with Main wings

b. Standard Model 2

The first modification made to the *Standard Model* was to change the minimum separation between the wings. This was accomplished by changing the length of the connecting rods holding the crankshaft to the flapping beams. This model was referred to as *Standard Model 2*, and has a minimum separation that was 22 mm less than the *Standard Model*. The plunge amplitude of the two models remained the same. An illustration of this model can be found in **Figure 21**. The main wings were kept attached when the model was tested in this configuration.

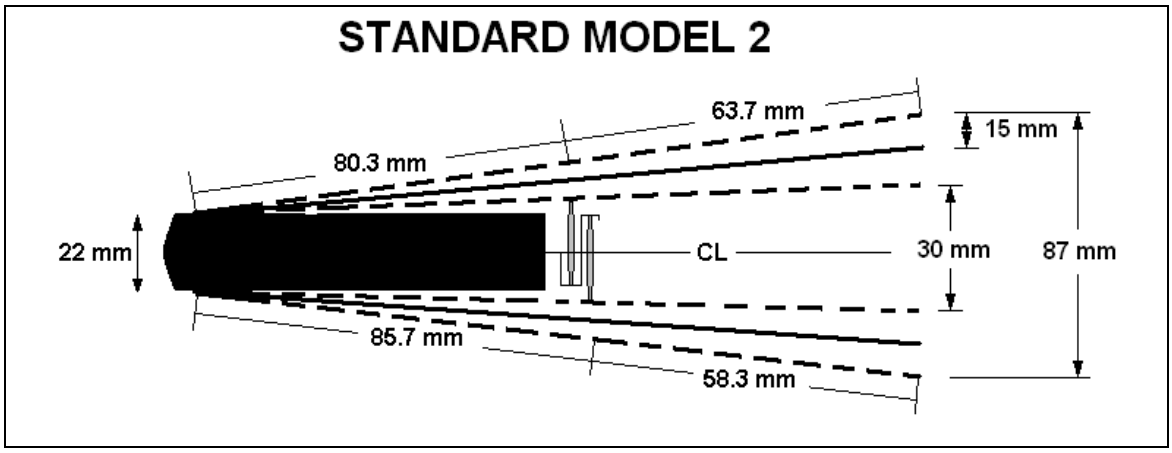

Figure 21. Standard Model 2 Schematic

c. Standard Model 3

The other modification made to the *Standard Model* was aimed at investigating the effects of plunge amplitude. The plunge amplitude was altered by switching out the crankshaft. *Standard Model 3* had a plunge amplitude that was 44% of the flapping wing chord. Manufacturing problems also resulted in a slight change in the mean separation. The new mean separation of *Standard Model 3* was 5.6 mm less than the *Standard Model.* A schematic of *Standard Model 3* can be seen in **Figure 22**. The main wings were kept attached when the model was tested in this configuration.

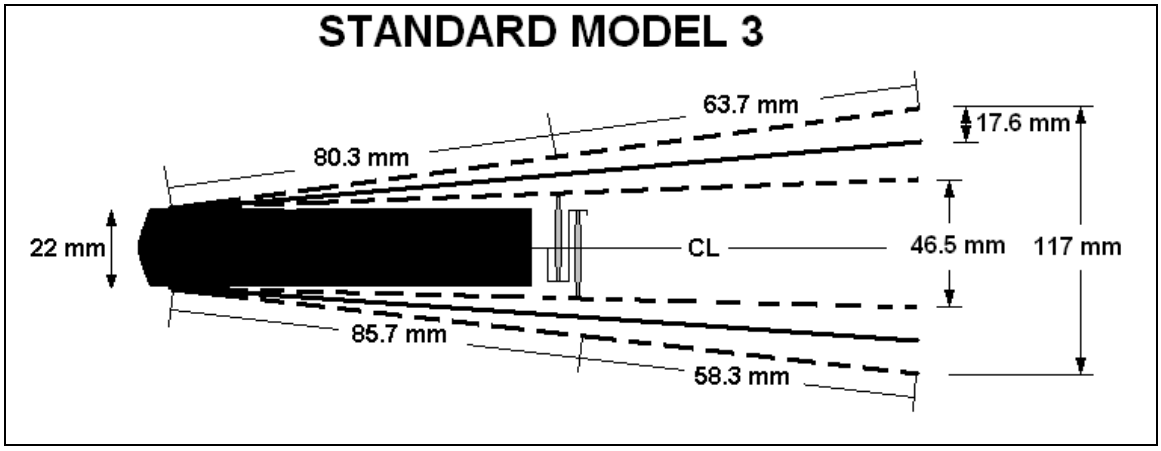

Figure 22. Standard Model 3 Schematic

C. DATA REDUCTION

1. Cycles

All of the data recorded for the various models was taken at a sample rate of 2000 HZ for 10 seconds. The data was analyzed using two MATLAB codes (**See Appendix A and B**). The codes were written so that the start and end of each cycle, as dictated by the square wave input, was found for each incoming data stream (the data streams being Channels 2, 3, 5 and 6 explained in the experimental setup). The average value over every cycle was then calculated for that particular data stream. Next, the mean of all the cycle averages was found for that sample. Finally, the mean of the five average sample values for each data set was used as the final value for that data stream. The standard deviation of the five mean sample values was used as the measurement error.

2. Figure of Merit

The figure of merit used to determine the static performance of the MAV was

$$FM = \frac{Grams \quad of \quad Thrust}{Shaft \quad Power} \tag{9}$$

This is a standard measure of performance used for many hovering type MAVs. It is important to note that the numerator in this equation is the *thrust available in a hovering state* divided by the acceleration of gravity. For the NPS MAV the thrust available in a hovering state is the net positive thrust created by the flapping wings.

3. Error Analysis

The measurements of lift and thrust each contained 4 primary sources of error. From the calibration process the slope error for both the lift and thrust channels

determined by equation (5) was on the order of machine precision and thus negligible. However, since the uncertainty of the average values found for each calibration data set in equation (4) was used to determine the slope error, this source of error needed to be included. Another source of uncertainty determined in the calibration process was the cross-talk between the lift and thrust channels. This turned out to be approximately 80% of the total error. One more source of error was the drift of the load cells during experimentation. Lastly, the standard deviation for each data set was included in the calculation for the uncertainty of the data set.

The only source of error involved in the frequency calculation was the standard deviation of the five average values found for each data set. This error was found to be the smallest out of all the measured data. For the worst case the frequency error was still only 0.2% of the actual value. Frequency error bars are left off of all subsequent plots as they are too small to be seen.

The error values calculated for the velocity measurements account for two uncertainties. The first is the change in offset from the time the tunnel is turned on until the time it is turned off. The actual offset used is the average of these two, but the error is taken as the full difference between the two data sets. The second source of error is the drift in velocity from the time the tunnel speed is set until it is changed again. It is during this interval that the data sets are recorded.

The uncertainty in the angle of attack is the same for all conditions and is dependent solely on the resolution of the angle finder. For these experiments the error was determined to be +/- 1 degree.

a. Error Calculation

The uncertainties listed above for each measurement were assumed to be independent of one another. Given this assumption, it is then feasible to calculate the error using a quadrature technique governed by the equation

$$error = \sqrt{\delta x^2 + \delta y^2 + \delta z^2 + \cdots} \qquad (10)$$

In this equation *dx*, *dy*, and *dz* all represent the sources of uncertainty in the measurement. Additional sources of error are added on accordingly.

THIS PAGE LEFT INTENTIONALLY BLANK

IV. EXPERIMENTAL RESULTS

A. MAV MOTOR

Previous MAV laboratory tests had measured the thrust production of the NPS MAV to be 9.5 grams using 1.5 Watts of electrical power. The efficiency of the MAV motor/gear-drive operating in this region was determined to be approximately 25% using Figure 17. Neglecting all other losses in the system other than the motor/gear-drive efficiency, these numbers provide a MAV Figure of Merit of **25 g/W**. All other hovering MAVs currently in production seem to operate at approximately 10 g/W [Ref. 15]. It can be clearly seen from these two numbers that the opposed-plunge, flapping-wing propulsion is much more effective at producing thrust.

B. STANDARD MODEL

The use of tapered wing shapes to eliminate spanwise oscillations of the flapping wings was a great aid to the controllability of the aircraft. It was desired to know whether this benefit in aircraft control had a detrimental effect to the thrust produced by the MAV. The MAV thrust is plotted in **Figures 23 and 24** as a function of flapping frequency for two different AOA and no freestream velocity using the *Standard Model* setup.

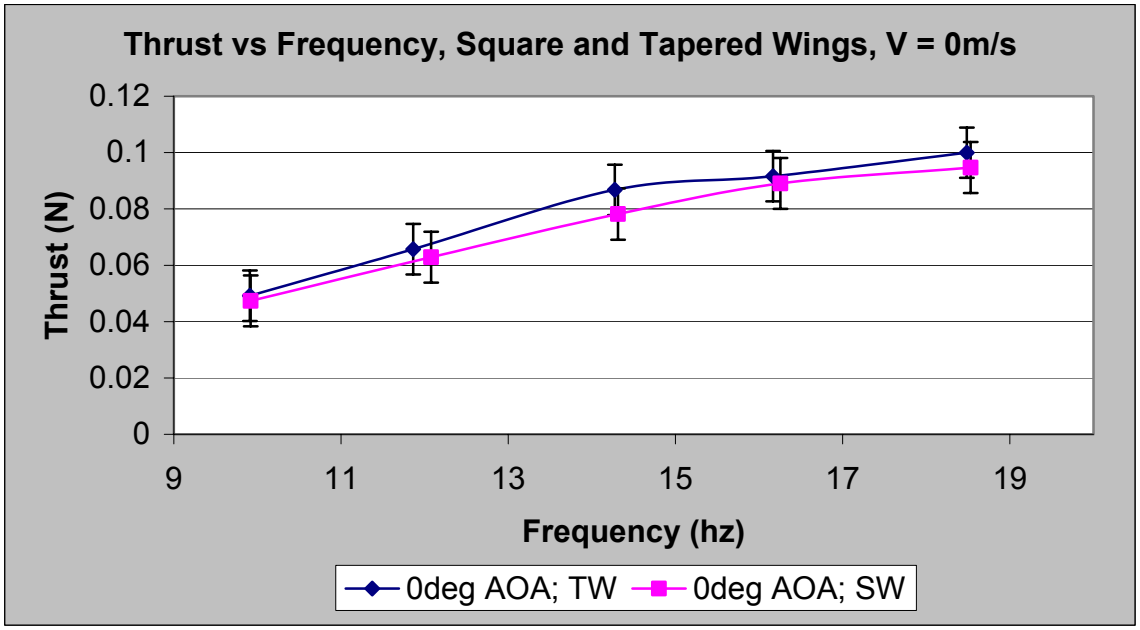

Figure 23. Thrust vs. Frequency, 0deg AOA, V=0 m/s, SM

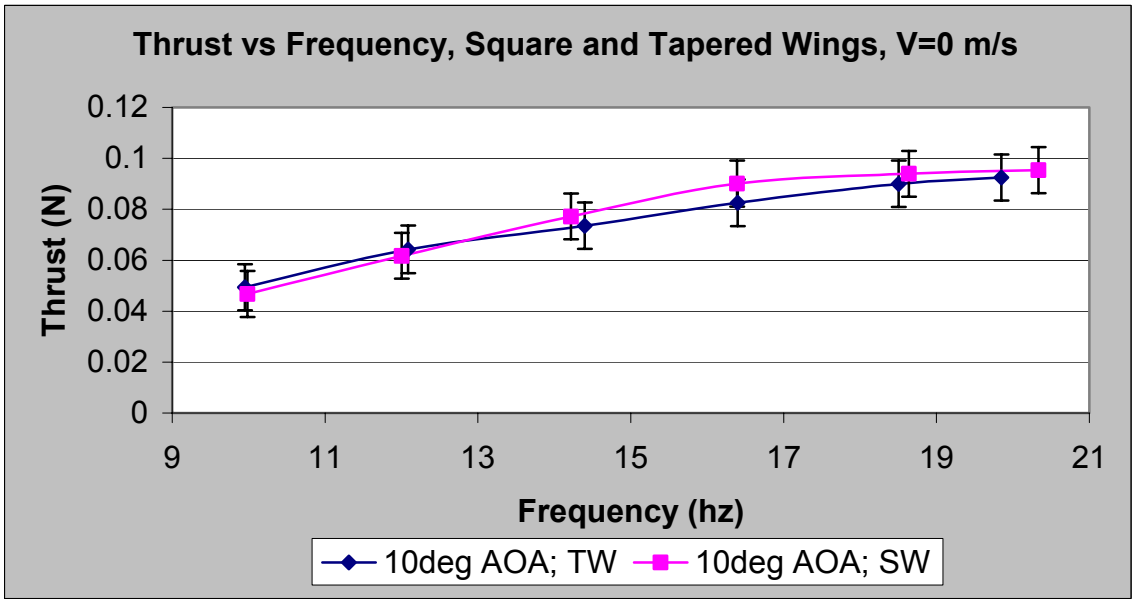

Figure 24. Thrust vs. Frequency, 10deg AOA, V=0 m/s, SM

Since the error bars overlapped for every data point in both graphs, and because the square and tapered wings alternated in each graph as to which was producing more thrust, it appeared that switching from a square to a

tapered flapping wing had a negligible on thrust production. This was not unreasonable as the amount of wing area lost due to tapering was only 8.3% of the total wing area for each wing.

The effects of AOA and freestream velocity on thrust production can be seen in **Figure 25**. In this graph thrust was plotted versus frequency using four different AOA and a freestream velocity of 4 m/s. This graph plainly shows that no significant change in thrust occurred from changing the AOA. Computer simulations of the Navier Stokes equations over similar setups also support these results [Ref. 12]. In addition, the adverse effect of increasing freestream velocity can be seen by comparing the thrust values for a given frequency in **Figure 25**, to the thrust values for the same frequency in **Figures 23 and 24**.

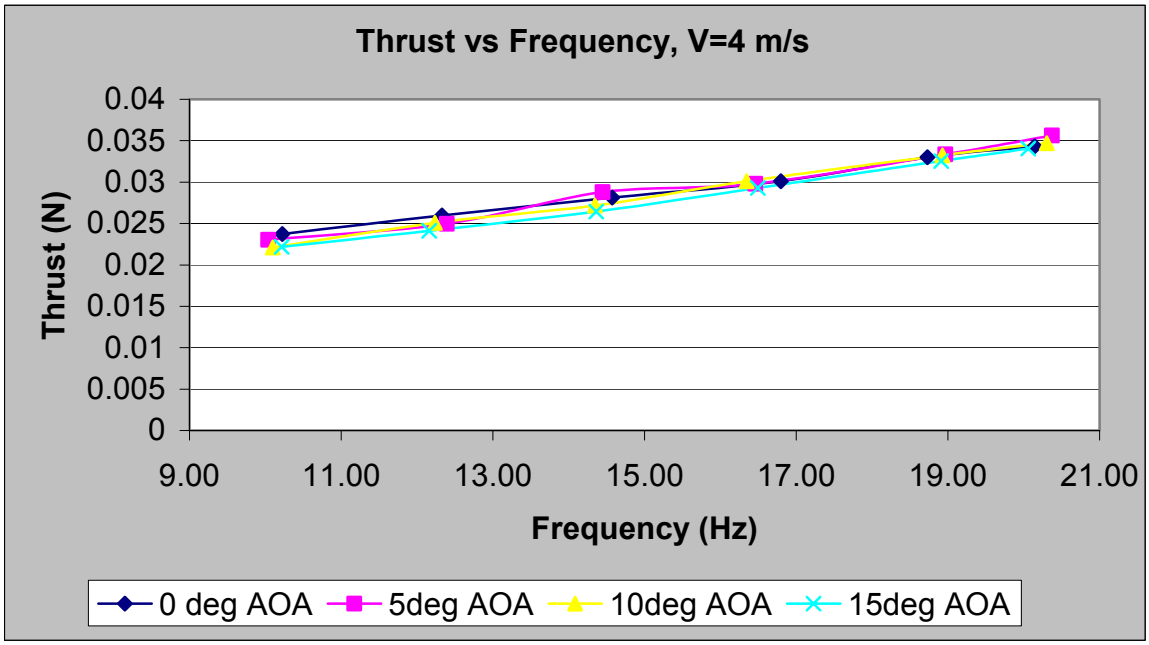

Figure 25. Thrust vs. Frequency, V=4 m/s, SM

C. STANDARD MODEL WITH MAIN WINGS

Attaching the main wings seemed to have a slight negative effect on the thrust being produced by the flapping wings(**See Figure 26 and 27**). This could possibly be a result of the upper flapping wing operating in the separated flow region behind the upper surface of the lifting wing. Although the trends on **Figure 26 and 27** are clear, because the error bars overlap the plotted lines, the statement that the main wings reduce thrust production can not be claimed for certain.

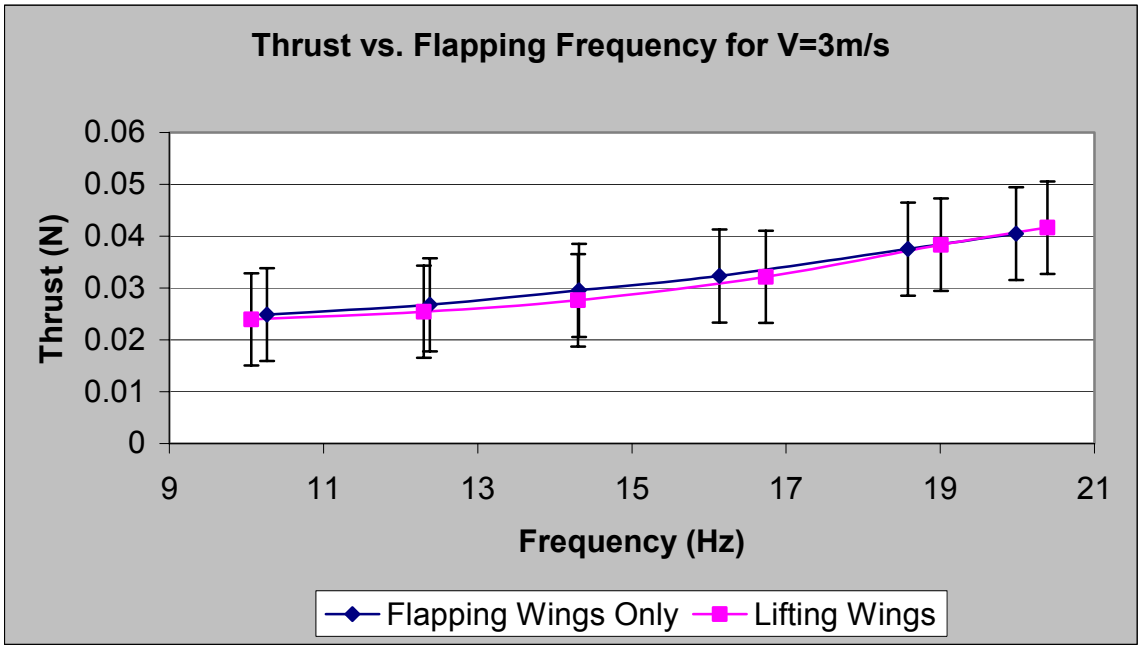

Figure 26. Thrust vs. Frequency, 0deg AOA, V=3 m/s, SM

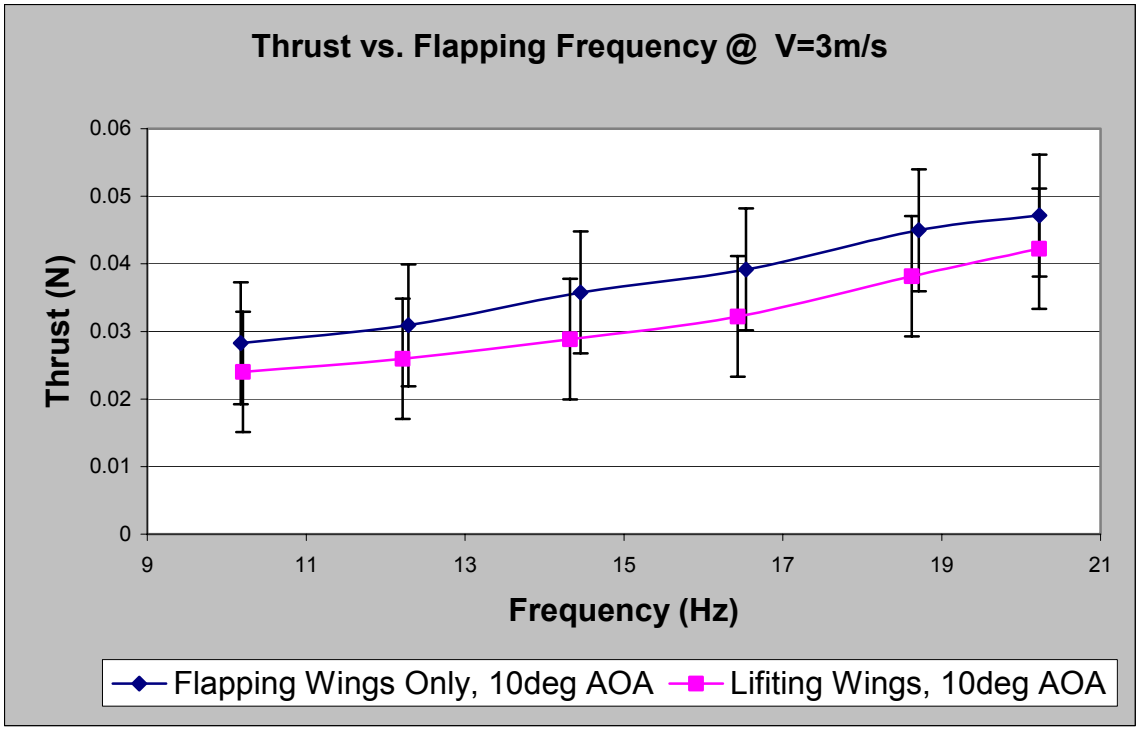

Figure 27. Thrust vs. Frequency, 10deg AOA, V=3 m/s, SM

D. STANDARD MODEL 2

Decreasing the minimum separation of the wings reduced the thrust that was produced. This effect can be clearly seen in **Figures 28 and 29**. In both of these graphs the thrust was seen to drop significantly from the Standard Model.

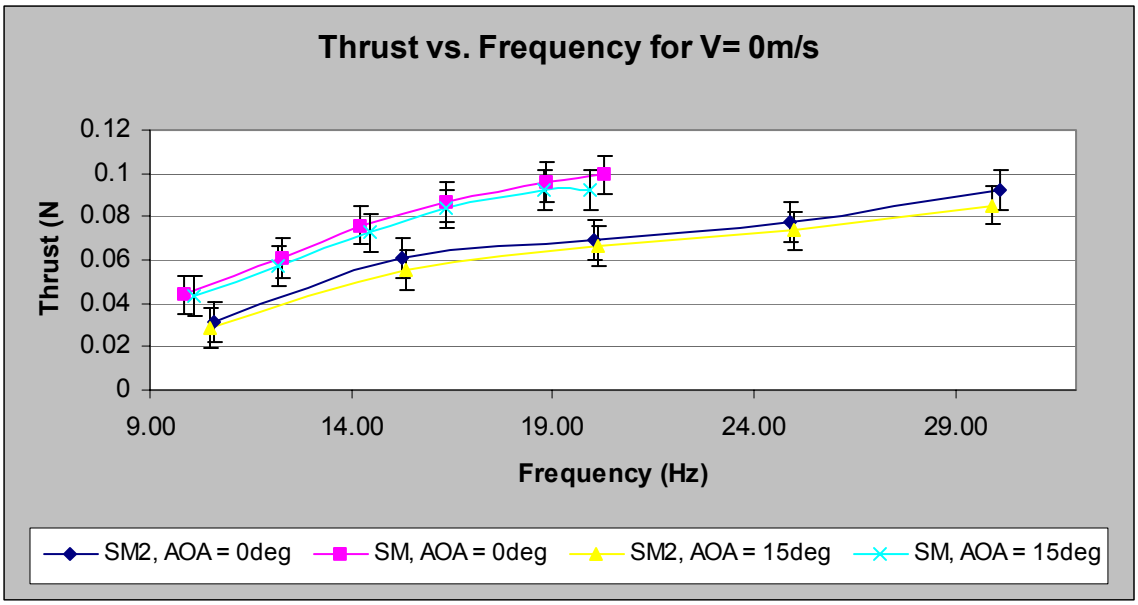

Figure 28. Thrust vs. Frequency, V=0 m/s, SM2

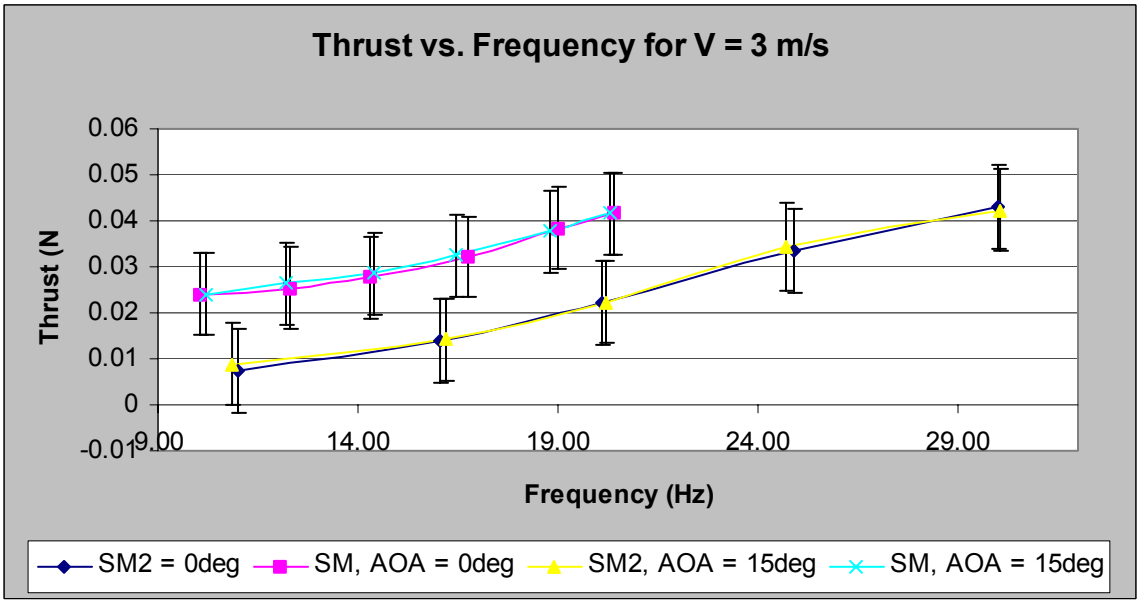

Figure 29. Thrust vs. Frequency, V= 3m/s, SM2

The trailing edges of the flapping wings were seen to collide with one another at the point of minimum separation in the flapping cycle. This occurrence seems a likely explanation for the loss of thrust production seen in going from the *Standard Model* to *Standard Model 2*. The collision prevented the flapping wings from feathering to

their natural positions and reducing the effective angle of attack. The effective angle of attack is too great without the feathering phenomenon, and as a result the flow separates off the flapping-wings and the thrust is diminished.

Alternatively, the lift was seen to increase dramatically when reducing the minimum separation (**See Figure 30**). The increase in lift was speculated to be a result of the flow remaining attached over the main wing. Flow visualization experiments were later conducted to test this theory. One possible explanation for why the flow remained attached can be justified by momentum conservation. If the flapping wings transfer some amount of momentum to the flow, then this momentum can be used to either accelerate the freestream to provide thrust, or to accelerate separated flow to increase lift. This theory could also account for some of the thrust losses seen in **Figure 29**. However, none of these theories can be substantiated at this juncture.

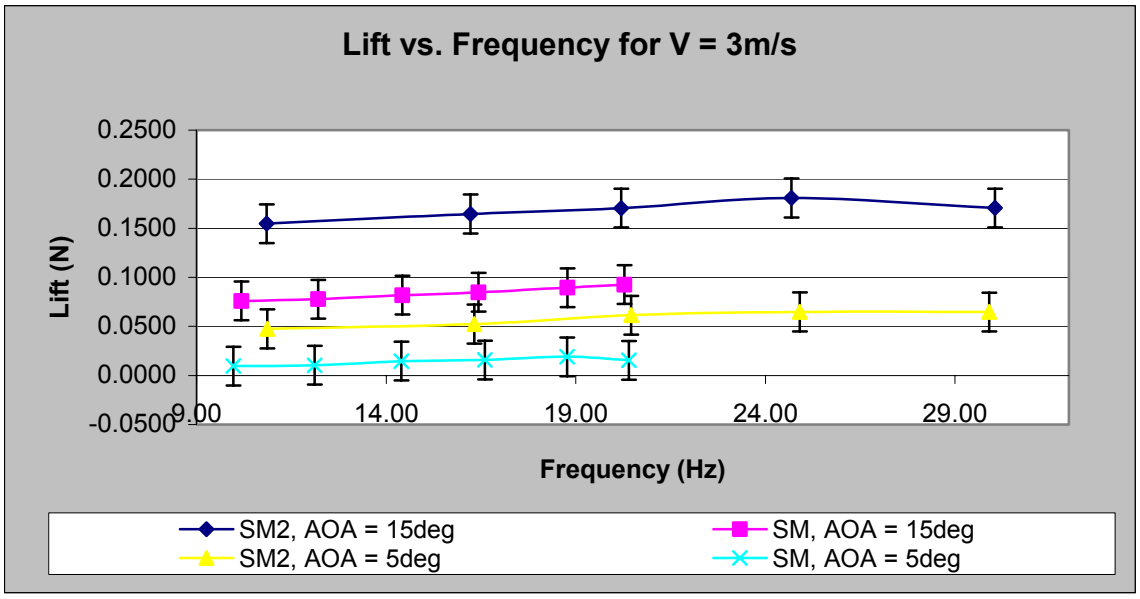

Figure 30. Lift vs. Frequency, V=3 m/s, SM2

E. STANDARD MODEL 3

The increase in plunge amplitude was predicted to increase the thrust produced by the flapping wings. However, the opposite effect was observed. Figures 31 and 32 illustrate this unexpected result.

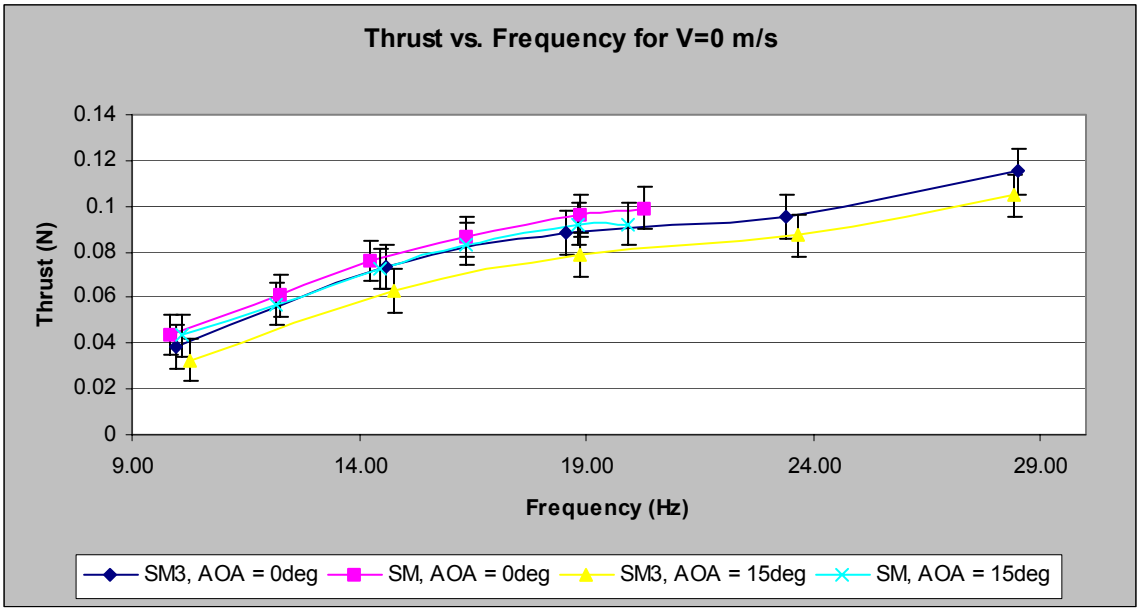

Figure 31. Thrust vs. Frequency, V=0 m/s, SM3

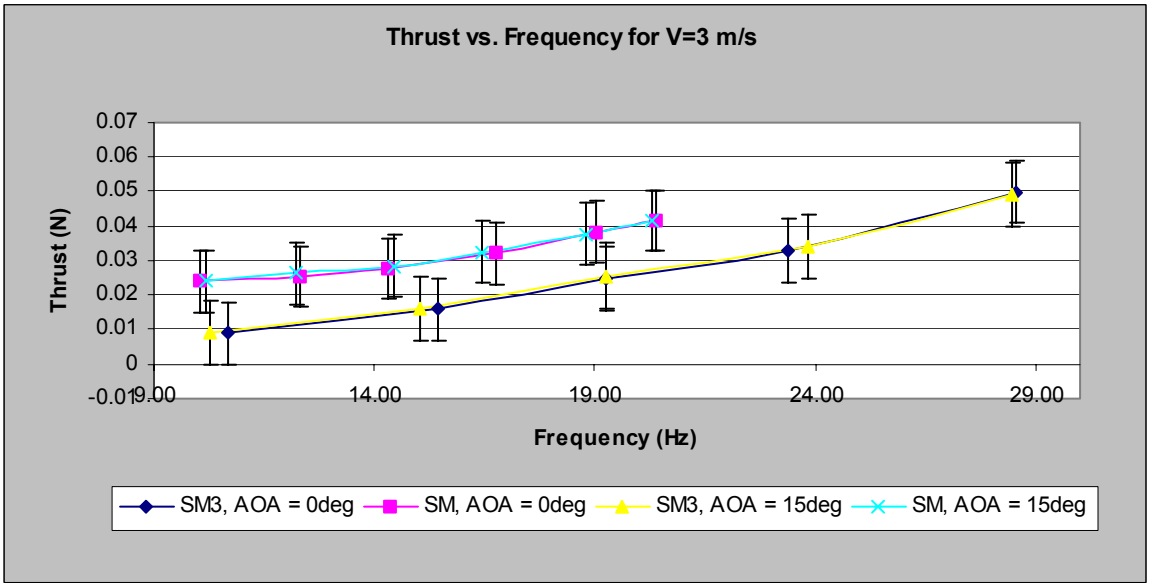

Figure 32. Thrust vs. Frequency, V=3 m/s, SM3

While intuitively it seemed that a greater swept out area during the flapping cycle would increase thrust, the elastic effects of the carbon fiber strip connecting the flapping wings to the flapping beams was not considered. The tendency of this connection was to allow the wing to pitch in the direction of the vertical motion in which it was traveling. Thus, at low freestream velocities such as in **Figure 31**, the effective angle of attack was reduced and a slight drop in performance between *Standard Model 3* and the *Standard Model* occurred. Conversely, at relatively fast velocities such as in **Figure 32**, the elasticity of the connection acted to increase the effective angle of attack, inviting separation and the associated loss in thrust. This phenomenon could also be another possible contribution to the thrust loss seen in the *Standard Model 2* experiments.

Furthermore, the fact that the *Standard Model* experiments provided greater amounts of thrust than the other two models suggested that the desired elasticity of the carbon-fiber strip changes with the plunge amplitude and mean separation of the flapping wings. In essence, the elasticity of the connection was not tuned well with the rest of the propulsion system for *Standard Model 2* and *3,* but was well tuned for the *Standard Model*. This fact points to the importance of the elasticity of the carbon fiber strip connections to the overall performance of the MAV.

The effects of *Standard Model 3* on the lift performance were somewhat unclear. The lift was found to dramatically increase with the changes made to this model(**See Figure 33**). However, it is unclear whether it was actually the increased plunge amplitude or the slight

reduction in minimum separation that achieved this result. As before, this improvement in lift was thought to be a result of the flow remaining attached over the main wing. Yet once again, the reason for this phenomenon has not yet been proved.

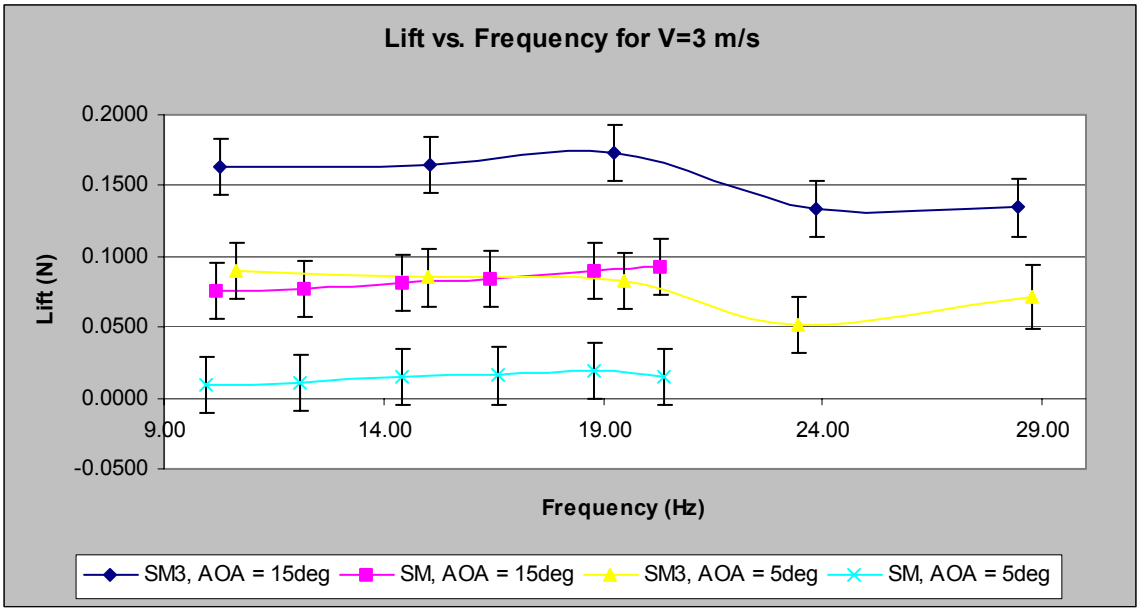

Figure 33. Lift vs. Frequency, V=3 m/s, SM3

One unexpected result was the dip in lift seen at the larger frequencies. This loss of lift was not seen in either of the other two models, and it is speculated that vibrations in the outside trailing edge of the main wing could be responsible (These vibrations were seen in the flow visualization experiments conducted). The fact that the drop in lift seems to be associated with frequency points to the possibility that the problem is related to damping and again suggests that the propulsion system is not tuned well for this model.

F. FLOW VISUALIZATION

A flow visualization experiment was carried out in order to confirm that the induced attachment of flow over the main wing from the flapping wings was the source of the increased lift seen in *Standard Model 2* and *3*. Streaklines were generated upstream of the MAV using a smoke wire and then recorded with digital video. The pictures presented here are taken from the digital video frames.

The first test case was the Standard Model. Video was taken of this model with the flapping on and off at an AOA of 15 degrees. In **Figure 34** one can clearly see that without any flapping at all the flow separated immediately after the leading edge.

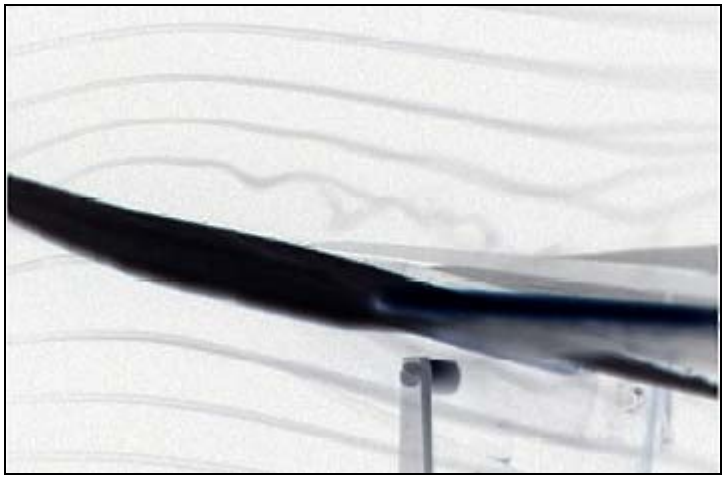

Figure 34. Flow Separation, V=2.0 m/s, 0 Hz, SM

Next, the flapping frequency was set to 31 Hz (**See Figure 35**). While the separation was not as extreme as in **Figure 34**, it can clearly be seen that the flow separates before reaching the end of the main wing.

Figure 35. Flow Separation, V=2.0 m/s, 31 Hz, SM

The second test case was *Standard Model 3*. The exact same experiment was carried out and the results are presented in **Figures 36 and 37**.

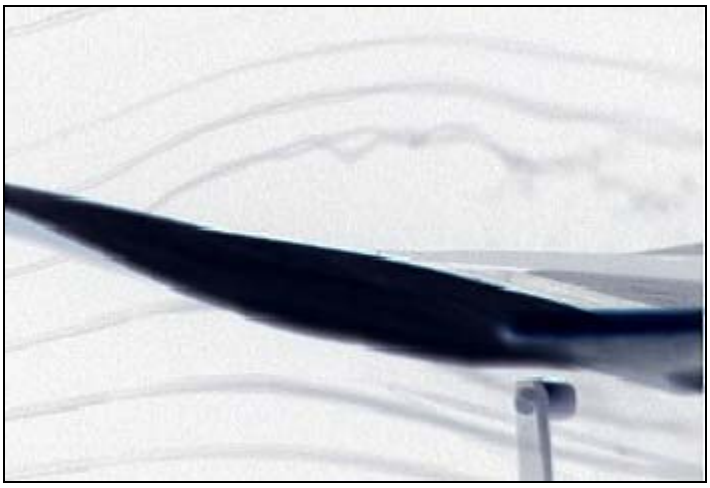

Figure 36. Flow Separation, V=2.0 m/s, 0 Hz, SM3

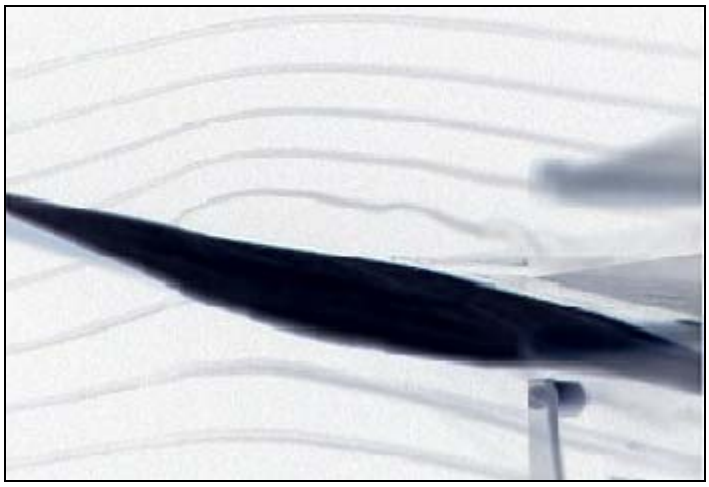

Figure 37. Flow Remains Attached, V=2.0 m/s, 31 Hz, SM3

In **Figure 36** it was again clear that the flow separates at a 15 degree AOA for this particular main wing shape with no flapping. However, when the flapping is activated in **Figure 37,** the first streakline above the leading edge of the main wing remains attached until the end of the main wing. It is then convected between the two flapping wings.

The fact that the flow remains attached over the surface of the main wing confirms the earlier stated theory that explained the reason for the increase in lift seen in *Standard Model 2* and *3*.

THIS PAGE INTENTIONALLY LEFT BLANK

V. CONCLUSIONS

The CIA and Special Forces groups have expressed interest in using MAVs for surveillance purposes for many years. Yet, it is because of the recent wars in Afghanistan and the Gulf that the need for MAVs in a combat environment has become clear. Current MAV models in production work well for some missions, but are limited because of undesirable characteristics such as noise and the inability to maneuver in confined spaces. The NPS MAV solves both of these problems through the employment of opposed-plunge flapping wings as the propulsion system.

Experimental testing of three different MAV models was carried out in the NPS 1.5 m x 1.5 m low-speed wind tunnel. One model was built to imitate the construction of the NPS flying MAV, and the other two changed the plunge amplitude and minimum separation, respectively, from the first model. Additionally, the motor efficiency and the effect of flapping wing shape were also studied. Lift and thrust forces acting on the MAV models were measured by sting-mounting the models on force balances. Flow visualization was also conducted on the models to validate theories developed to explain model performance.

Certain deductions became apparent after the experimental data had been evaluated. These included:

1. Opposed-pitch flapping wing propulsion was at least twice as effective at producing thrust than other current hovering MAVs. This was evidenced by the great improvement in MAV figure of merit for the NPS MAV model over other MAV models.

2. The tapered flapping wings used on the NPS MAV have no measurable effect on thrust production and reduce spanwise oscillations of the flapping wings.

3. Thrust was not sensitive to AOA changes between 0 and 15 degrees.

4. Thrust was very sensitive to velocity changes, with increases in velocity diminishing thrust production.

5. One possible contribution to the reduced thrust production seen in *Standard Model 2* and 3 is increased effective angles of attack that are too great for the flapping wings.

6. The increase in lift seen when mean separation is reduced can not be definitely attributed to the decrease in mean separation. Most likely a secondary effect caused by the reduction in mean separation is responsible for entraining the flow.

7. The dramatic increase in lift seen in *Standard Model 2* and *3* as compared with the *Standard Model* was a result of inducing the flow to stay attached over the entire main wing surface. This theory was confirmed with flow visualization techniques.

VI. RECOMMENDATIONS

The negative effects on thrust production made from changing the geometric characteristics of the MAV propulsion system could possibly stem from the elastic properties of the connection between the flapping wing and the flapping beam. While this property was not considered for this paper, undoubtedly the significance of this parameter has been demonstrated. Perhaps a helpful study would be to quantify the effects of elasticity on thrust production as a function of the geometric characteristics of the MAV propulsion system.

THIS PAGE INTENTIONALLY LEFT BLANK

APPENDIX A. MATLAB CODE FOR CALCULATING EXPERIMENTAL OFFSET VALUES

```
clear all
%BEGIN NESTED FOR LOOP CALCULATIONS; LOAD DATA SETS
%USE ZERO SPEED AND ZERO FLAPPING FILE TO SET OFFSETS, THEN USE AT ZERO
FLAPPING AT EACH SPPED TO OBTAIN PROFILE DRAG ESTIMATES
offset_data =  []
for z = 0:4
    x       = 'load';
    eval([x ' ' 'off0100' num2str(z) '.txt']);

    %INITIALIZE VARIABLES
    data     = zeros(20000,1);
    data     = eval(['off0100' num2str(z)]);
    lift     = zeros(20000,1);
    lift     = data(:,2);
    thrust   = zeros(20000,1);
    thrust   = data(:,3);

    %FIND AVEGARE VALUES
    liftavg     = 0;
    liftavg     = mean(lift);
    thrustavg   = 0;
    thrustavg   = mean(thrust);

    %SAVE DATA TO FILE
    test_data     = 0;
    test_data     = [liftavg, thrustavg];
    offset_data   = [test_data; offset_data];
    clear data;
    clear eval(['off1100' num2str(z)]);
end

for z = 0:4
    x       = 'load';
    eval([x ' ' 'off0200' num2str(z) '.txt']);

    %INITIALIZE VARIABLES
    data     = zeros(20000,1);
    data     = eval(['off0200' num2str(z)]);
    lift     = zeros(20000,1);
    lift     = data(:,2);
    thrust   = zeros(20000,1);
    thrust   = data(:,3);

    %FIND AVEGARE VALUES
    liftavg     = 0;
    liftavg     = mean(lift);
    thrustavg   = 0;
    thrustavg   = mean(thrust);

    %SAVE DATA TO FILE
    test_data     = 0;
```

```
    test_data     = [liftavg, thrustavg];
    offset_data   = [test_data; offset_data];
    clear data;
    clear eval(['off1200' num2str(z)]);
end

offsets     = mean(offset_data);
lift_off    = offsets(1)
thrust_off  = offsets(2)
```

APPENDIX B. MATLAB CODE FOR CALCULATING EXPERIMENTAL THRUST AND LIFT VALUES

```
clear all
LT_offset

% INPUT VALUES FROM PRE-FLIGHT ANALYSIS
veloccal        = 133.2;
rhoair          = 1.225;
velocvolts      = 0.0;
vinf            = ((velocvolts*veloccal)/(0.5*rhoair))^(0.5);
b               = .250;
c               = .040;
plunge_amp      = 0.017625;

%VALUES FROM CALIBRATION EXPERIMENTS
liftcal         =  -0.00015651;
thrustcal       = 5.7349e-005;

%BEGIN NESTED FOR LOOP CALCULATIONS; LOAD DATA SETS
w           =  [35,50,63,76,92];
flight_data =  []

for yy = 1:5
    for zz = 0:4
        xx       = 'load';
        eval([xx ' ' 'pa0' num2str(w(yy)) '00' num2str(zz) '.txt']);

        %INITIALIZE VARIABLES
        data    = zeros(20000,1);
        data    = eval(['pa0' num2str(w(yy)) '00' num2str(zz)]);
        lift    = zeros(20000,1);
        lift    = (((data(:,2) - lift_off).*liftcal));
        thrust  = zeros(20000,1);
        thrust  = ((data(:,3) - thrust_off).*thrustcal);

        %FIND CYCLE START AND END INDICES
        fbl     = 0;
        fbl     = 900;
        freq    = 0;
        freq    = ge(data(:,1),fbl);
        d       = 0;
        d       = find(freq);
        m       = 0;
        q       = 0;
        [m,q]   = size(d);
        e       = zeros(m,1);
        e(1)    = d(1);
        i       = 0;

        for i = 2:m
            if [(d(i)-d(i-1)) > 1.5]
                e(i,1) = d(i);
            elseif [(d(i)-d(i-1)) == 1]
```

```
        e(i,1) = 0;
    end
end

%FIND ROTATIONAL SPEED
f       = 0;
g       = 0;
h       = 0;
[f,g,h] = find(e);
p       = 0;
r       = 0;
[p,r]   = size(h);
k       = 0;
time    = 0;

for k=2:p-1
    time(k-1,1) = h(k+1)-h(k);
end

timeperrev = 0;
timeperrev = time(:,1).*(0.0005);
RPS        = 0;
RPS        = 1./timeperrev;
omega      = 0;
omega      = RPS*2*3.142; %(rad/s)

%FIND AVERAGE VALUES PER CYCLE
j          = 0;
avgliftv   = 0;
avgthrustv  = 0;

for j = 2:p-1
    avgliftv(j-1,1)=sum(lift(h(j):(h(j+1)-1)))/((h(j+1)-1)-
    h(j));
    avgthrustv(j-1,1)=sum(thrust(h(j):(h(j+1)-1)))/((h(j+1)-1)-
    h(j));
end

%FIND AVEGARE VALUES
liftavg     = 0;
liftavg     = mean(avgliftv);
thrustavg   = 0;
thrustavg   = mean(avgthrustv);
omegaavg    = 0;
omegaavg    = mean(omega);

%CALCULATE COEFFICEINTS AND EFFICIENCIES
freqavg     = 0;
freqavg     = (omegaavg/(2*3.142));
refveloc   = 0;
refveloc   = sqrt(vinf^2 + (2*3.142*freqavg*plunge_amp)^2);
coeffthrust = 0;
coeffthrust = (thrustavg)/(4*plunge_amp*b*rhoair*(refveloc)^2);
coefflift   = 0;
coefflift   = (liftavg)/(4*plunge_amp*b*rhoair*(refveloc)^2);
```

```
        %SAVE DATA TO FILE
        test_data     = 0;
        test_data          =  [freqavg,  refveloc,  liftavg,  thrustavg,
coeffthrust, coefflift];
        flight_data   = [test_data; flight_data];
        clear data;
        clear eval(['ms0' num2str(w(yy)) '00' num2str(zz)]);
    end
end

save offset_data offset_data
```

THIS PAGE INTENTIONALLY LEFT BLANK

APPENDIX C. EXPERIMENTAL DATA FOR STANDARD MODEL WITH LIFTING WINGS

SMLW

AOA = 0deg	Freqavg	Lift	Thrust	T_ERROR	L_ERROR
Vinf = 0 m/s	20.26	-0.05102	0.09926	0.00891	0.01972
	18.86	-0.05092	0.09586	0.00898	0.01972
	16.35	-0.0514	0.0866	0.00903	0.01972
	14.24	-0.052	0.07612	0.00900	0.01972
	12.26	-0.0542	0.0609	0.00906	0.01976
	9.83	-0.05754	0.04386	0.00891	0.01972
Vinf = 1.00 m/s	20.16	-0.04856	0.07966	0.00902	0.01972
	18.97	-0.04854	0.07602	0.00896	0.01973
	16.45	-0.0495	0.06522	0.00910	0.01972
	14.37	-0.0485	0.05272	0.00896	0.01979
	12.16	-0.04936	0.03938	0.00896	0.01972
	9.99	-0.04864	0.02832	0.00896	0.01975
Vinf = 2.03 m/s	20.39	-0.03376	0.05796	0.00900	0.01972
	18.91	-0.03308	0.05248	0.00900	0.01972
	16.60	-0.03536	0.04242	0.00900	0.01976
	14.70	-0.03518	0.0354	0.00903	0.01973
	12.55	-0.03658	0.02758	0.00900	0.01974
	10.31	-0.03658	0.02342	0.00900	0.01974
Vinf = 3.00 m/s	20.39	-0.01622	0.04164	0.00890	0.01973
	19.01	-0.01538	0.03836	0.00890	0.01974
	16.74	-0.02036	0.03218	0.00890	0.01974
	14.30	-0.01906	0.02764	0.00891	0.01972
	12.30	-0.02242	0.02542	0.00890	0.01974
	10.06	-0.02632	0.02394	0.00889	0.01989
Vinf = 4.03 m/s	20.14	-0.00138	0.0343	0.00891	0.02060
	18.73	-0.00996	0.033	0.00891	0.01973
	16.80	-0.01072	0.0301	0.00892	0.01976
	14.57	-0.00982	0.02814	0.00891	0.01973
	12.33	-0.00954	0.02598	0.00894	0.01974
	10.22	-0.00936	0.02374	0.00891	0.01972

SMLW

AOA = 5deg	Freqavg	Lift	Thrust	T_ERROR	L_ERROR
Vinf = 0 m/s	20.24	-0.0605	0.09598	0.00901	0.01972
	18.69	-0.0656	0.0935	0.00897	0.01972
	16.35	-0.0662	0.08466	0.00900	0.01972
	14.10	-0.0675	0.07284	0.00897	0.01972
	12.11	-0.0678	0.05792	0.00897	0.01973
	9.80	-0.0760	0.04264	0.00897	0.01972
Vinf = 1.08 m/s	20.22	-0.0522	0.07892	0.00893	0.01972
	18.64	-0.0540	0.0727	0.00892	0.01973
	16.54	-0.0568	0.06232	0.00899	0.01972

	14.40	-0.0588	0.05036	0.00892	0.01973
	12.46	-0.0601	0.03866	0.00892	0.01972
	10.33	-0.0607	0.02886	0.00892	0.01972
Vinf = 2.06 m/s	20.37	-0.0177	0.05674	0.00890	0.01973
	18.71	-0.0191	0.05054	0.00890	0.01975
	16.48	-0.0209	0.04304	0.00892	0.01972
	14.54	-0.0216	0.03434	0.00891	0.01980
	12.04	-0.0263	0.02666	0.00890	0.01972
	9.87	-0.0307	0.02348	0.00890	0.01975
Vinf = 3.01 m/s	20.40	0.0155	0.04302	0.00916	0.01973
	18.77	0.0191	0.0388	0.00916	0.01975
	16.60	0.0157	0.0334	0.00918	0.01986
	14.40	0.0146	0.0291	0.00917	0.01974
	12.12	0.0105	0.02642	0.00916	0.01972
	9.97	0.0097	0.0245	0.00916	0.01973
Vinf = 4.00 m/s	20.37	0.0554	0.03562	0.00910	0.01994
	18.97	0.0540	0.03334	0.00912	0.01989
	16.46	0.0541	0.0298	0.00914	0.01978
	14.45	0.0507	0.02878	0.00911	0.01974
	12.39	0.0477	0.02498	0.00944	0.02105
	10.04	0.0486	0.02302	0.00911	0.01973

SMLW

AOA = 10deg

	Freqavg	**Lift**	**Thrust**	**T_ERROR**	**L_ERROR**
Vinf = 0 m/s	20.24	-0.0491	0.09632	0.00890	0.01973
	18.57	-0.0500	0.0916	0.00891	0.01972
	16.26	-0.0511	0.08442	0.00894	0.01973
	14.47	-0.0524	0.0747	0.00890	0.01972
	11.92	-0.0568	0.05726	0.00891	0.01973
	9.78	-0.0598	0.04196	0.00891	0.01974
Vinf = 0.99 m/s	20.21	-0.0396	0.0833	0.01294	0.02047
	18.83	-0.0388	0.07446	0.00891	0.01973
	16.54	-0.0388	0.06428	0.00892	0.01972
	14.45	-0.0420	0.0573	0.01378	0.02065
	12.19	-0.0461	0.04338	0.01379	0.02094
	10.01	-0.0450	0.0288	0.00891	0.01972
Vinf = 1.97 m/s	20.01	0.0069	0.05694	0.00915	0.01973
	18.80	0.0052	0.05242	0.00915	0.01972
	16.55	0.0079	0.04386	0.00917	0.01973
	14.39	0.0070	0.03512	0.00915	0.01977
	12.13	0.0049	0.0286	0.00915	0.01975
	10.24	0.0030	0.02436	0.00915	0.01975
Vinf = 3.05 m/s	20.23	0.0681	0.04224	0.00891	0.01974
	18.62	0.0713	0.03816	0.00891	0.01973
	16.43	0.0720	0.03222	0.00928	0.01973
	14.32	0.0688	0.02886	0.00892	0.01972
	12.21	0.0667	0.02596	0.00892	0.01999
	10.21	0.0616	0.02402	0.00891	0.01972
Vinf = 4.01 m/s	20.30	0.1408	0.03472	0.00890	0.01974
	18.93	0.1331	0.03322	0.00890	0.01988

	16.35	0.1330	0.0301	0.00892	0.01976
	14.35	0.1288	0.02716	0.00891	0.01983
	12.24	0.1279	0.02508	0.00890	0.01972
	10.10	0.1340	0.0221	0.00890	0.01975

SMLW

AOA = 15deg					
	Fregavg	**Lift**	**Thrust**	**T_ERROR**	**L_ERROR**
Vinf = 0 m/s	19.93	-0.0640	0.09218	0.00891	0.01972
	18.81	-0.0667	0.09208	0.00905	0.01974
	16.36	-0.0688	0.08356	0.00912	0.01972
	14.45	-0.0705	0.07268	0.00890	0.01972
	12.16	-0.0748	0.0572	0.00891	0.01977
	10.09	-0.0822	0.04338	0.00889	0.01974
Vinf = 1.00 m/s	20.13	-0.0467	0.07714	0.00890	0.01973
	18.87	-0.0487	0.0729	0.00890	0.01973
	16.57	-0.0510	0.06288	0.00891	0.01973
	14.19	-0.0538	0.05076	0.00890	0.01972
	12.36	-0.0553	0.0398	0.00890	0.01973
	9.93	-0.0567	0.02866	0.00890	0.01972
Vinf = 2.03 m/s	20.17	0.0139	0.05548	0.00891	0.01975
	18.70	0.0108	0.05048	0.00891	0.01974
	16.35	0.0098	0.04242	0.00894	0.01973
	14.57	0.0081	0.03524	0.00892	0.01972
	12.21	0.0090	0.0283	0.00891	0.01972
	9.95	0.0052	0.024	0.00892	0.01973
Vinf = 3.02 m/s	20.28	0.0926	0.04156	0.00893	0.01972
	18.78	0.0895	0.03776	0.00891	0.01972
	16.43	0.0848	0.03246	0.00903	0.01978
	14.42	0.0818	0.02854	0.00893	0.01973
	12.21	0.0778	0.02636	0.00891	0.01974
	10.18	0.0760	0.02412	0.00891	0.01974
Vinf = 4.03 m/s	20.06	0.1966	0.03404	0.00894	0.01975
	18.91	0.1911	0.03256	0.00895	0.01992
	16.49	0.1843	0.02928	0.00900	0.01973
	14.36	0.1828	0.02644	0.00896	0.01982
	12.16	0.1818	0.02412	0.00895	0.01973
	10.22	0.1806	0.0222	0.00894	0.01973

THIS PAGE INTENTIONALLY LEFT BLANK

APPENDIX D. EXPERIMENTAL DATA FOR STANDARD MODEL 2

SM2

AOA = 0deg

	Freqavg	Lift	Thrust	T_ERROR	L_ERROR
Vinf = 0 m/s	30.10	0.00645	0.09195	0.00922	0.01979
	24.90	-0.01668	0.07754	0.00924	0.01974
	20.00	-0.02151	0.06960	0.00922	0.01972
	15.24	-0.02130	0.06124	0.00931	0.01972
	10.60	-0.02238	0.03123	0.00922	0.01972
Vinf = 0.99 m/s	30.01	-0.00784	0.07937	0.00896	0.01990
	24.89	0.01147	0.06860	0.00896	0.01973
	19.59	0.02481	0.05694	0.00897	0.01973
	15.56	0.02208	0.04294	0.00896	0.01972
	10.85	0.02111	0.01635	0.00896	0.01972
Vinf = 2.02 m/s	29.90	0.02499	0.06115	0.00897	0.02060
	24.43	0.00009	0.04842	0.00904	0.01979
	19.78	0.00058	0.03624	0.00897	0.01974
	15.60	0.00552	0.02121	0.00897	0.01977
	10.72	0.00419	0.00672	0.00897	0.01979
Vinf = 3.02 m/s	30.02	0.02467	0.04320	0.00913	0.01980
	24.92	0.02917	0.03341	0.00913	0.01998
	20.08	0.02949	0.02212	0.00913	0.01985
	16.05	0.03003	0.01405	0.00913	0.01979
	10.99	0.02769	0.00751	0.00913	0.01988
Vinf = 4.01 m/s	30.24	0.02074	0.03040	0.00895	0.02094
	24.90	0.02360	0.02470	0.00894	0.01988
	20.57	0.01659	0.01843	0.00894	0.01982
	16.04	0.01803	0.01333	0.00893	0.02031
	10.86	0.01431	0.00718	0.00894	0.01989

SM2

AOA = 5deg

	Freqavg	Lift	Thrust	T_ERROR	L_ERROR
Vinf = 0 m/s	29.95	-0.00141	0.08946	0.00904	0.02159
	24.87	0.00704	0.07841	0.00909	0.01973
	19.99	0.00942	0.06993	0.00905	0.01974
	15.27	0.00710	0.05982	0.00904	0.01973
	10.25	0.00196	0.02867	0.00922	0.01972
Vinf = 1.00 m/s	29.85	0.04721	0.07776	0.00894	0.02154
	24.93	0.01788	0.06603	0.00895	0.01977
	19.96	0.01674	0.05597	0.00894	0.01973
	15.57	0.01186	0.04045	0.00894	0.01978
	10.90	0.00860	0.01571	0.00894	0.01973
Vinf = 2.02 m/s	30.52	0.03585	0.06110	0.00917	0.01981
	24.30	0.06527	0.04592	0.00917	0.01978
	20.29	0.06427	0.03636	0.00916	0.01994
	15.92	0.06015	0.02139	0.00916	0.01974
	11.38	0.05808	0.00763	0.00917	0.01973
Vinf = 3.02 m/s	29.90	0.06467	0.04181	0.00896	0.01974

	24.90	0.06479	0.03240	0.00897	0.01986
	20.46	0.06146	0.02288	0.00899	0.01979
	16.33	0.05247	0.01468	0.00897	0.01991
	10.86	0.04750	0.00773	0.00896	0.01983
Vinf = 4.01 m/s	30.24	0.09382	0.03052	0.00936	0.02025
	25.16	0.08349	0.02450	0.00936	0.02121
	20.55	0.08228	0.01857	0.00936	0.01978
	16.47	0.07747	0.01488	0.00937	0.02030
	10.74	0.07565	0.00773	0.00936	0.01998

SM2

AOA = 10deg

	Freqavg	Lift	Thrust	T_ERROR	L_ERROR
Vinf = 0 m/s	29.95	-0.00832	0.08685	0.00892	0.02642
	24.92	0.01345	0.07522	0.00897	0.01974
	19.96	0.01595	0.06882	0.00894	0.01973
	15.08	0.01237	0.05680	0.00892	0.01975
	10.76	0.00556	0.03017	0.00903	0.01973
Vinf = 0.95 m/s	29.85	0.01297	0.07714	0.00905	0.02506
	24.70	0.02653	0.06570	0.01059	0.01972
	20.21	0.02583	0.05691	0.00905	0.01977
	15.46	0.02244	0.04162	0.00905	0.01973
	11.07	0.01407	0.01855	0.00905	0.01980
Vinf = 1.99 m/s	30.32	0.10018	0.05982	0.00894	0.01981
	24.84	0.10904	0.04832	0.00894	0.01976
	20.16	0.10528	0.03663	0.00894	0.01974
	15.92	0.10631	0.02219	0.00893	0.01973
	11.41	0.10531	0.00818	0.00893	0.01976
Vinf = 3.03 m/s	30.21	0.14465	0.04233	0.00898	0.01973
	24.91	0.15400	0.03304	0.00900	0.01975
	20.22	0.15029	0.02213	0.00898	0.01972
	16.39	0.14759	0.01494	0.00898	0.01974
	11.11	0.14785	0.00784	0.00898	0.01981
Vinf = 4.02 m/s	30.13	0.21011	0.03037	0.00890	0.02018
	25.29	0.21123	0.02423	0.00891	0.01988
	20.71	0.21430	0.01805	0.00891	0.01977
	16.32	0.21041	0.01368	0.00890	0.01973
	10.89	0.20114	0.00742	0.00890	0.02013

SM2

AOA = 15deg

	Freqavg	Lift	Thrust	T_ERROR	L_ERROR
Vinf = 0 m/s	29.90	0.03225	0.08520	0.00898	0.02542
	24.97	0.04313	0.07344	0.00898	0.01972
	20.12	0.04529	0.06631	0.00896	0.01976
	15.38	0.04201	0.05541	0.00891	0.01972
	10.48	0.03081	0.02849	0.00892	0.01976
Vinf = 0.94 m/s	30.31	0.01474	0.07668	0.00919	0.02346
	25.11	0.02496	0.06389	0.00921	0.01985
	20.10	0.01767	0.05507	0.00919	0.01972
	15.74	0.01375	0.04039	0.00920	0.01975
	10.72	0.00362	0.01500	0.00919	0.01975

Vinf = 2.01 m/s	30.38	0.09122	0.05712	0.00899	0.01973
	24.88	0.09707	0.04465	0.00901	0.01999
	20.02	0.09003	0.03360	0.00898	0.01974
	15.87	0.08761	0.02024	0.00898	0.01980
	10.87	0.08234	0.00653	0.00898	0.01972
Vinf = 3.0 m/s	30.05	0.17071	0.04224	0.00892	0.01974
	24.69	0.18079	0.03431	0.00945	0.01984
	20.20	0.17051	0.02231	0.00892	0.01976
	16.22	0.16455	0.01434	0.00892	0.01991
	10.84	0.15476	0.00884	0.00893	0.01972
Vinf = 3.98 m/s	30.39	0.26620	0.03169	0.00911	0.01988
	25.17	0.27513	0.02456	0.00911	0.01989
	20.75	0.26442	0.01905	0.00911	0.01989
	16.74	0.25625	0.01490	0.00911	0.01974
	11.47	0.25180	0.00977	0.00911	0.01976

THIS PAGE INTENTIONALLY LEFT BLANK

APPENDIX E. EXPERIMENTAL DATA FOR STANDARD MODEL 3

SMLW

AOA = 0deg	Freqavg	Lift	Thrust	T_ERROR	L_ERROR
Vinf = 0 m/s	20.26	-0.05102	0.09926	0.00891	0.01972
	18.86	-0.05092	0.09586	0.00898	0.01972
	16.35	-0.0514	0.0866	0.00903	0.01972
	14.24	-0.052	0.07612	0.00900	0.01972
	12.26	-0.0542	0.0609	0.00906	0.01976
	9.83	-0.05754	0.04386	0.00891	0.01972
Vinf = 1.00 m/s	20.16	-0.04856	0.07966	0.00902	0.01972
	18.97	-0.04854	0.07602	0.00896	0.01973
	16.45	-0.0495	0.06522	0.00910	0.01972
	14.37	-0.0485	0.05272	0.00896	0.01979
	12.16	-0.04936	0.03938	0.00896	0.01972
	9.99	-0.04864	0.02832	0.00896	0.01975
Vinf = 2.03 m/s	20.39	-0.03376	0.05796	0.00900	0.01972
	18.91	-0.03308	0.05248	0.00900	0.01972
	16.60	-0.03536	0.04242	0.00900	0.01976
	14.70	-0.03518	0.0354	0.00903	0.01973
	12.55	-0.03658	0.02758	0.00900	0.01974
	10.31	-0.03658	0.02342	0.00900	0.01974
Vinf = 3.00 m/s	20.39	-0.01622	0.04164	0.00890	0.01973
	19.01	-0.01538	0.03836	0.00890	0.01974
	16.74	-0.02036	0.03218	0.00890	0.01974
	14.30	-0.01906	0.02764	0.00891	0.01972
	12.30	-0.02242	0.02542	0.00890	0.01974
	10.06	-0.02632	0.02394	0.00889	0.01989
Vinf = 4.03 m/s	20.14	-0.00138	0.0343	0.00891	0.02060
	18.73	-0.00996	0.033	0.00891	0.01973
	16.80	-0.01072	0.0301	0.00892	0.01976
	14.57	-0.00982	0.02814	0.00891	0.01973
	12.33	-0.00954	0.02598	0.00894	0.01974
	10.22	-0.00936	0.02374	0.00891	0.01972

SMLW

AOA = 5deg	Freqavg	Lift	Thrust	T_ERROR	L_ERROR
Vinf = 0 m/s	20.24	-0.06046	0.09598	0.00901	0.01972
	18.69	-0.06564	0.09350	0.00897	0.01972
	16.35	-0.06620	0.08466	0.00900	0.01972
	14.10	-0.06754	0.07284	0.00897	0.01972
	12.11	-0.06780	0.05792	0.00897	0.01973
	9.80	-0.07598	0.04264	0.00897	0.01972
Vinf = 1.08 m/s	20.22	-0.05218	0.07892	0.00893	0.01972
	18.64	-0.05404	0.07270	0.00892	0.01973
	16.54	-0.05676	0.06232	0.00899	0.01972
	14.40	-0.05876	0.05036	0.00892	0.01973
	12.46	-0.06010	0.03866	0.00892	0.01972

	10.33	-0.06070	0.02886	0.00892	0.01972
Vinf = 2.06 m/s	20.37	-0.01774	0.05674	0.00890	0.01973
	18.71	-0.01912	0.05054	0.00890	0.01975
	16.48	-0.02094	0.04304	0.00892	0.01972
	14.54	-0.02164	0.03434	0.00891	0.01980
	12.04	-0.02626	0.02666	0.00890	0.01972
	9.87	-0.03068	0.02348	0.00890	0.01975
Vinf = 3.01 m/s	20.40	0.01548	0.04302	0.00916	0.01973
	18.77	0.01910	0.03880	0.00916	0.01975
	16.60	0.01574	0.03340	0.00918	0.01986
	14.40	0.01458	0.02910	0.00917	0.01974
	12.12	0.01046	0.02642	0.00916	0.01972
	9.97	0.00966	0.02450	0.00916	0.01973
Vinf = 4.00 m/s	20.37	0.05544	0.03562	0.00910	0.01994
	18.97	0.05402	0.03334	0.00912	0.01989
	16.46	0.05414	0.02980	0.00914	0.01978
	14.45	0.05068	0.02878	0.00911	0.01974
	12.39	0.04766	0.02498	0.00944	0.02105
	10.04	0.04862	0.02302	0.00911	0.01973

SMLW

AOA = 10deg	Freqavg	Lift	Thrust	T_ERROR	L_ERROR
Vinf = 0 m/s	20.24	-0.04906	0.09632	0.00890	0.01973
	18.57	-0.05002	0.09160	0.00891	0.01972
	16.26	-0.05112	0.08442	0.00894	0.01973
	14.47	-0.05240	0.07470	0.00890	0.01972
	11.92	-0.05678	0.05726	0.00891	0.01973
	9.78	-0.05978	0.04196	0.00891	0.01974
Vinf = 0.99 m/s	20.21	-0.03964	0.08330	0.01294	0.02047
	18.83	-0.03876	0.07446	0.00891	0.01973
	16.54	-0.03878	0.06428	0.00892	0.01972
	14.45	-0.04196	0.05730	0.01378	0.02065
	12.19	-0.04608	0.04338	0.01379	0.02094
	10.01	-0.04504	0.02880	0.00891	0.01972
Vinf = 1.97 m/s	20.01	0.00690	0.05694	0.00915	0.01973
	18.80	0.00522	0.05242	0.00915	0.01972
	16.55	0.00786	0.04386	0.00917	0.01973
	14.39	0.00700	0.03512	0.00915	0.01977
	12.13	0.00492	0.02860	0.00915	0.01975
	10.24	0.00300	0.02436	0.00915	0.01975
Vinf = 3.05 m/s	20.23	0.06810	0.04224	0.00891	0.01974
	18.62	0.07128	0.03816	0.00891	0.01973
	16.43	0.07204	0.03222	0.00928	0.01973
	14.32	0.06880	0.02886	0.00892	0.01972
	12.21	0.06668	0.02596	0.00892	0.01999
	10.21	0.06156	0.02402	0.00891	0.01972
Vinf = 4.01 m/s	20.30	0.14082	0.03472	0.00890	0.01974
	18.93	0.13306	0.03322	0.00890	0.01988
	16.35	0.13302	0.03010	0.00892	0.01976
	14.35	0.12884	0.02716	0.00891	0.01983

	12.24	0.12786	0.02508	0.00890	0.01972
	10.10	0.13398	0.02210	0.00890	0.01975

SMLW

AOA = 15deg	Freqavg	Lift	Thrust	T_ERROR	L_ERROR
Vinf = 0 m/s	19.93	-0.06396	0.09218	0.00891	0.01972
	18.81	-0.06674	0.09208	0.00905	0.01974
	16.36	-0.06876	0.08356	0.00912	0.01972
	14.45	-0.07046	0.07268	0.00890	0.01972
	12.16	-0.07478	0.05720	0.00891	0.01977
	10.09	-0.08218	0.04338	0.00889	0.01974
Vinf = 1.00 m/s	20.13	-0.04666	0.07714	0.00890	0.01973
	18.87	-0.04874	0.07290	0.00890	0.01973
	16.57	-0.05098	0.06288	0.00891	0.01973
	14.19	-0.05378	0.05076	0.00890	0.01972
	12.36	-0.05528	0.03980	0.00890	0.01973
	9.93	-0.05668	0.02866	0.00890	0.01972
Vinf = 2.03 m/s	20.17	0.01388	0.05548	0.00891	0.01975
	18.70	0.01078	0.05048	0.00891	0.01974
	16.35	0.00982	0.04242	0.00894	0.01973
	14.57	0.00810	0.03524	0.00892	0.01972
	12.21	0.00898	0.02830	0.00891	0.01972
	9.95	0.00522	0.02400	0.00892	0.01973
Vinf = 3.02 m/s	20.28	0.09256	0.04156	0.00893	0.01972
	18.78	0.08950	0.03776	0.00891	0.01972
	16.43	0.08480	0.03246	0.00903	0.01978
	14.42	0.08182	0.02854	0.00893	0.01973
	12.21	0.07776	0.02636	0.00891	0.01974
	10.18	0.07600	0.02412	0.00891	0.01974
Vinf = 4.03 m/s	20.06	0.19660	0.03404	0.00894	0.01975
	18.91	0.19110	0.03256	0.00895	0.01992
	16.49	0.18432	0.02928	0.00900	0.01973
	14.36	0.18282	0.02644	0.00896	0.01982
	12.16	0.18176	0.02412	0.00895	0.01973
	10.22	0.18058	0.02220	0.00894	0.01973

THIS PAGE INTENTIONALLY LEFT BLANK

LIST OF REFERENCES

1. Francis, M.S. and McMichael, J.M., “Micro Air Vehicles - Towards a New Dimension in Flight,” www.darpa.mil/tto/MAV/mav_auvsi.htm, August 7,2002.

2. Grasmeyer, M.J. and Keenon, M.T., “Development of the Black Widow Micro Air Vehicle,” AIAA Paper No. 2001-0127, Simi Valley, California, January 2001.

3. Grossman, J., “The Buzzzz at Caltech, Something New in Southern California’s Skies,” Los Angeles Times Magazine, December 10, 2000, p. 8.

4. Knoller, R., “Die Gesetze des Luftwiderstandes,” *Flug- und Motortechnik* (Wien), Vol. 3, No. 21, 1909, pp. 1-7.

5. Betz, A., “Ein Beitrag zur Erklarung des Segelfluges,” *Zeitschrift fur Flugtechnik und Motorluftschiffahrt*, Vol. 3, January. 1912, pp. 269-272.

6. Katzmayr, R., “Effect of Periodic Changes of Angle of Attack on Behavior of Airfoils,” NACA Report No. 147, Oct. 1922 (translated from *Zeitschrift fur Flugtechnik und Motorluftschiffart*, March 31, 1922, pp.80-82, and April 13, 1922, pp. 95-101).

7. Birnbaum, W., “Das ebene Problem des schlagenden Fluels,” *Zeitschrift fur Angewandte Mathematik und Mechanik*, Vol. 4, No. 4, August, 1924, pp 277-292.

8. Birnbaum, W., “Der Schlagflugelpropeller und die kleinen Schwingungen elastich befestigter Tragflugel,” Zeitschrift fur Flugtechnik und Motorluftschiffahrt, Vol. 15, 1924, pp. 128-134.

9. Von Karman, T. and Burgers, J.M., “General Aerodynamic Theory – Perfect Fluids,” Division E, Vol. II, Aerodynamic Theory, Ed. Durand, W.F., 1943, p. 308.

10. Garrick, I.E., “Propulsion of a Flapping and Oscillating Airfoil,” NACA Report 567, 1936.

11. Schmidt, W., “Der Wellpropeller, ein neuer Antrieb fuer Wasser-, Land-, und Luftfahrzeuge,” Z. Flugwiss. Vol. 13, 1965, pp. 472-479.

12. Jones, K.D., Castro, B.M., Mahmoud, O., and Platzer, M.F., “A Numerical and Experimental Investifation of Flapping Wing Propulsion in Ground Effect,” AIAA Paper No. 2002-0866, Reno, Nevada, January 2002.

13. Jones, K.D., and Platzer, M.F., “Experimental Investigation of the Aerodynamic Characterisitcs of Flapping-Wing Micro Air Vehicles,” AIAA Paper No. 2003-0418, Reno, Nevada, January 2003.

14. Duggan, S.J., *An Experimental Investigation of Flapping-Wing Propulsion for Micro Air Vehicles.* Master’s Thesis. Naval Postgraduate School. Monterey, California. June 2000.

15. Young, L.A., et. al, “Use of Vertical Lift Planetary Aerial Vehicles for the Exploration of Mars.” [http://www.lpi.usra.edu/meetings/robomars/pdf/6227.pdf]. June, 2003.

INITIAL DISTRIBUTION LIST

1. Defense Technical Information Center
   Ft. Belvoir, Virginia

2. Dudley Knox Library
   Naval Postgraduate School
   Monterey, California

3. Prof. Kevin D. Jones, Code AA/Jo
   Naval Postgraduate School
   Monterey, California

4. Prof. Max F. Platzer, Code AA/Pl
   Naval Postgraduate School
   Monterey, California

5. Prof. Arthur Schoenstadt
   Naval Postgraduate School
   Monterey, California

6. Ens Jason N. Papadopoulos
   Naval Postgraduate School
   Monterey, California

7. Nicholas Papadopoulos
   Mary Esther, Florida

8. Ens Jonas B. Kelsall
   Seal Team Seven
   Coronado, California